



UNIVERSITEIT • STELLENBOSCH • UNIVERSITY
jou kennisvenoot • your knowledge partner

Design, build and test a passive thermal system for a loft

A roof solar chimney application for South African weather conditions

Lauren Margaret Beviss-Challinor

Project report presented in partial fulfilment of the requirements for the degree of
Master of Engineering at the University of Stellenbosch

December 2007



Departement Meganiese en Megatroniese Ingenieurswese
Department of Mechanical and Mechatronic Engineering



Design, build and test a passive thermal system for a loft

A roof solar chimney application for South African weather conditions

Masters of Engineering Project

Lauren Margaret Beviss-Challinor
Department of Mechanical Engineering
Stellenbosch University

Supervisor: RT Dobson

Final Report

December 2007

EXECUTIVE SUMMARY

The design, construction and testing of a passive thermal system, a roof solar chimney, for a loft is considered. Unlike conventional solar chimneys the solar collector is constructed from corrugated iron roof sheets with the aim that it can be integrated into existing buildings at a lower costs or used in low cost housing developments. The main objective of the study was to determine the feasibility of such low-cost design to regulate thermal conditions in a loft, that is heating the loft during winter and enhancing natural ventilation during summer, by carrying out an experimental and analytical study.

The results obtained from the experimental study showed that for winter the solar chimney, having a channel width, depth and length of 0.7 m, 0.1 m and 1.8 m respectively and with a peak solar radiation of 850 W/m^2 , heated the room air $5 \text{ }^\circ\text{C}$ higher than the ambient temperature during the hottest periods of the day, which is only marginally better than a loft with conventional roof insulation. At night, it was found that reverse airflow occurred through the chimney, cooling the loft down to ambient temperature, due to radiation heat loss from the roof collector to the night sky. For summer operation, the experimental data showed that the chimney was able to maintain the loft at ambient temperature and the analytical study found that the chimney was able to enhance natural ventilation effectively, reaching air exchange rate of 6.6 per hour for the 4.6 m^3 volume space. It was also found that the chimney's performance dropped rapidly and significantly during periods of low solar radiation and at night. A sensitivity analysis illustrated that for both summer and winter operation, the size, tilt angle and absorptivity of the roof collector greatly effected the efficiency and mass flow rates of the system, agreeing well with other literature.

These results prove that this low cost solar chimney cooling design was feasible to enhance natural ventilation mainly during hot summer conditions with high solar radiation. Compared to a loft with only conventional roof insulation, the chimney did not perform effectively during the winter to heat the loft up, meaning that winter operation for this specific design is not feasible. Possible improvements to the design include using construction materials with higher thermal capacities to retain heat

energy and ensure continued operation during periods of low solar radiation, as well as using selective absorber coatings on the collector surface. It is recommended that further work on the project include the integration of these improvements into the present design and to use the findings obtained from the sensitivity analysis to improve system efficiencies. CFD analysis of the test-rig will be insightful as an additional means to validate and compare with the analytical and experimental data obtained in this report.

With the continuation of these studies, this low-cost solar chimney design can be optimised, validated on a commercial scale and built into existing and new housing developments. Incorporating such a passive thermal device will aid homeowners in air regulation and thermal comfort of their living space as well as saving on energy requirements.

DECLARATION

I, the undersigned, hereby declare that the work contained in this assignment is my own original work and that I have not previously in its entirety or in part submitted it at any university for a degree.

Signed

Date

ACKNOWLEDGEMENTS

The author would like to thank Mr Clive September and Mr Cobus Zietsman for the construction and supervision of the test-rig.

TABLE OF CONTENTS

| | Page |
|--|-------------|
| Executive summary..... | i |
| Declaration..... | iii |
| Acknowledgements..... | iv |
| Nomenclature..... | vii |
| List of figures..... | x |
| List of tables..... | xii |
| 1 Introduction..... | 1-1 |
| 2 Objectives | 2-3 |
| 3 Literature review | 3-7 |
| 4 Experimental work..... | 4-10 |
| 4.1 Design and construction of test-rig..... | 4-10 |
| 4.2 Operation..... | 4-14 |
| 4.2.1 Summer conditions | 4-14 |
| 4.2.2 Winter conditions..... | 4-14 |
| 4.3 Instrumentation | 4-15 |
| 4.4 Results..... | 4-17 |
| 4.4.1 Winter operation | 4-17 |
| 4.4.2 Summer operation..... | 4-19 |
| 5 Analytical study | 5-20 |
| 5.1 Thermal model..... | 5-20 |
| 5.1.1 Winter | 5-21 |
| 5.1.2 Summer..... | 5-30 |
| 5.2 Computer program..... | 5-34 |
| 5.3 Results..... | 5-36 |
| 5.3.1 Winter | 5-36 |
| 5.3.2 Summer..... | 5-38 |
| 5.4 Sensitivity analysis..... | 5-42 |

| | | |
|-------|---|------|
| 5.4.1 | Winter | 5-42 |
| 5.4.2 | Summer | 5-44 |
| 6 | Discussion and conclusions | 6-46 |
| 7 | Recommendations..... | 7-50 |
| 8 | References..... | 8-52 |
| | Appendix A: Thermal functions and calculations | A-1 |
| | Appendix B: Time dependent input functions for computer program | B-1 |
| B.1 | Winter program input functions..... | B-1 |
| B.2 | Summer program input functions | B-4 |
| | Appendix C: Radiation effects | C-1 |
| | Appendix D: Data CD containing computer simulation programs | D-1 |

NOMENCLATURE

| | |
|-----------|--|
| A | surface area, m^2 |
| A_c | cross-sectional area, m^2 |
| C_f | friction factor |
| C_p | constant pressure specific heat, kJ/kg K |
| C_v | constant volume specific heat, kJ/kg K |
| ds | roof thickness, m |
| D | diameter, m |
| D_{hyd} | hydraulic diameter, m |
| DX | channel control volume length, m |
| DY | channel control volume depth, m |
| DZ | channel control volume width, m |
| g | gravitational acceleration, m/s^2 |
| G | incident solar radiation, W/m^2 |
| h | convection heat coefficient, $W/m^2 \text{ } ^\circ\text{C}$ |
| k | thermal conductivity, $W/m \text{ } ^\circ\text{C}$ |
| L | length, m |
| L_{eq} | equivalent length, m |
| m | mass, kg |
| \dot{m} | mass flow rate, kg/s |
| N | number of control volumes |
| Nu | Nusselt number |
| P | pressure, Pa |
| Pr | Prandtl number |
| Q | total heat transfer, kJ |
| \dot{Q} | heat transfer rate, W |
| R | gas constant, kJ/kg K |
| Ra | Raleigh number |
| Re | Reynold's number |
| t | time, s |
| t | thickness, m |
| T | temperature, $^\circ\text{C}$ or K |

| | |
|-----|------------------------|
| v | velocity, m/s |
| V | volume, m ³ |

Greek

| | |
|--------------------------|--|
| α | absorptivity |
| β | volume expansivity, 1/K |
| ΔP | pressure drop, Pa |
| ΔT | temperature difference, °C or K |
| Δt | time period, s |
| ε | emissivity |
| ζ | solar insolation geometric factor |
| $\eta_{thermal}$ | thermal efficiency for winter operation |
| $\eta_{flow\ enhancing}$ | flow enhancing efficiency for summer operation |
| θ | roof inclination angle, ° |
| μ | dynamic viscosity, kg/ms or Ns/m ² |
| ρ | density, kg/m ³ |
| σ | Stefan-Boltzmann constant |
| τ | shear stress, N/m ² |
| ν | kinematic viscosity, m ² /s |
| ϕ | relative humidity |
| ψ | sun azimuth angle, ° |
| ω | sun altitude angle, ° |

Subscripts

| | |
|--------|---------------|
| abs | absorption |
| avg | average |
| b | bottom |
| conduc | conduction |
| convec | convection |
| down | below surface |
| dp | dewpoint |

| | |
|-------|---------------------------|
| e | ambient conditions |
| f | roof |
| i | i^{th} component |
| in | flowing in |
| m | channel |
| out | flowing out |
| r | space or room |
| room | space or room |
| s | insulation |
| s | side |
| s | summer |
| t_1 | start time |
| t_2 | end time |
| up | above surface |
| w | winter |

Superscripts

| | |
|---------|------------------------|
| \cdot | quantity per unit time |
| $-$ | average |

LIST OF FIGURES

| | |
|--|------|
| Figure 1.1: Solar chimney as part of the exterior wall of a building | 1-3 |
| Figure 2.1: Sketch of conventional chimney design..... | 2-4 |
| Figure 2.2: Sketch of proposed chimney design..... | 2-4 |
| Figure 2.3: Principle of roof solar chimney concept..... | 2-5 |
| Figure 4.1: Proposed test-rig showing three separate compartments | 4-11 |
| Figure 4.2: Construction of the solar chimney's lower section | 4-12 |
| Figure 4.3: Test-rig built on site | 4-13 |
| Figure 4.4: Expected operation of test-rig during summer | 4-14 |
| Figure 4.5: Expected operation of test-rig during winter..... | 4-15 |
| Figure 4.6: Placement of temperature sensors in the test-rig..... | 4-16 |
| Figure 4.7: Weather station set up near test-rig | 4-16 |
| Figure 4.8: Two typical sunny days in winter..... | 4-17 |
| Figure 4.9: Two typical cloudy days in winter | 4-18 |
| Figure 4.10: Two typical days in summer | 4-20 |
| Figure 5.1: Most important parameters of winter analytical model..... | 5-22 |
| Figure 5.2: Control volume for roof section | 5-23 |
| Figure 5.3: Sketch of air channel control volume..... | 5-25 |
| Figure 5.4: Sketch of room control volume | 5-27 |
| Figure 5.5: Law of momentum applied to one control volume | 5-28 |
| Figure 5.6: Most important parameters of summer analytical model..... | 5-31 |
| Figure 5.7: Sketch of summer room control volume | 5-32 |
| Figure 5.8: Simulation program results for a sunny day in Winter | 5-36 |
| Figure 5.9: Simulation program results for a cloudy day in Winter | 5-37 |
| Figure 5.10: Mass flow rate and incident solar radiation for winter operation..... | 5-38 |
| Figure 5.11: Three simulation models for summer operation comparison..... | 5-38 |
| Figure 5.12: Simulation program results for a typical sunny day in summer..... | 5-39 |
| Figure 5.13: Mass flow rates for summer operation..... | 5-41 |
| Figure 6.1: Comparison of experimental and analytical data for winter operation . | 6-46 |
| Figure 6.2: Comparison of experimental and analytical data for summer operation | 6-48 |
| Figure B.1: Incident solar radiation on a horizontal plate in winter (sunny day) | B-1 |
| Figure B.2: Incident solar radiation on a horizontal plate in winter (cloudy day)..... | B-2 |
| Figure B.3: Solar Radiation Geometric factor ζ_w for winter | B-2 |

| | |
|--|------|
| Figure B.4: Ambient air temperature over 24 hours | B-3 |
| Figure B.5: Relative Humidity over 24 hours..... | B-3 |
| Figure B.6: Wind speed over 24 hours | B-3 |
| Figure B.7: Incident solar radiation on a horizontal plate for summer..... | B-4 |
| Figure B.8: Solar Radiation Geometric factor ζ_s for summer | B-4 |
| Figure B.9: Ambient air temperature for a typical day in summer..... | B-5 |
| Figure B.10: Relative humidity over 24 hours..... | B-5 |
| Figure B.11: Wind speed over 24 hours | B-5 |
| Figure C.1: Model for basis of radiation heat transfer calculation | C-1 |
| Figure C.2: Cross section of box for radiation effect calculations | C-2 |
| Figure C.3: Resistance network for radiation model | C-3 |
| Figure C.4: Thermal model for polystyrene box | C-5 |
| Figure C.5: Wall inner boundary control volume..... | C-6 |
| Figure C.6: Wall outer boundary control volume..... | C-7 |
| Figure C.7: Inner control volume of wall | C-8 |
| Figure C.8: Results for radiation heat transfer effects | C-10 |

LIST OF TABLES

| | |
|--|------|
| Table 5.1: Input values for computer program | 5-35 |
| Table 5.2: Sensitivity analysis results for winter operation..... | 5-43 |
| Table 5.3: Sensitivity analysis results for summer operation | 5-45 |

1 INTRODUCTION

Thermal comfort is a very important aspect in our daily lives. Up until now thermal comfort was mostly achieved using mechanical means such as heaters and air conditioners which require large amounts of energy input, while in the developing countries, charcoal and other more crude forms of fossil fuels are burned for warmth, which is both detrimental to the environment and to people's health. In light of today's increasing energy shortages, rising oil prices and concerns for the environment however, more emphasis has been towards passive means of achieving comfort levels, mostly mainly through the increased use of passive thermal systems in architectural styles to suit the relevant environment.

Passive thermal systems use natural ventilation as a means of transferring heat from a building to the environment, through vents in the walls. Ultimately, the success of ventilation would then depend on air change rates in order to regulate the room's temperature. Bansal *et al.* (1993) describes the effect of ventilation caused by thermal forces and emphasises that in order for sufficient air changes per day to occur one of two conditions must be met: there must either be a substantial difference between the indoor and outdoor temperatures or there must be a large vertical distance between the vents to ensure a pressure difference to induce air flow.

Harnessing solar energy is one method of inducing large temperature and density differences between the outside environment and the inner building envelope, resulting in appreciable airflow changes. Solar energy is particularly suited because of its complimentary nature: the hotter the weather the more solar energy is available for absorption and the larger the temperature differences and induced air-change rates.

The rate of incident solar radiation in South Africa is one of the highest in the world, confirmed by the Renewable Energy Annual (1995): "the annual 24 hour global solar radiation average is about 220 W/m² for South Africa, compared to about 150 W/m² for parts of the United States and about 100 W/m² for Europe and the U.K.", yet little effort has gone into harnessing this energy for our thermal comfort needs. With mostly clear skies all year round, South Africa's potential for using solar energy in

both summer and winter is substantial, which could improve the country's energy, social and environmental problems in a sustainable manner.

There are many methods of using solar energy for passive thermal applications. One of the most popular of these systems is the concept of the solar chimney used for enhancing natural ventilation or inducing air changes through a living area using solar energy as input power.

Usually, solar chimneys are built vertically as part of the exterior walls of a building, and are therefore a premeditated design forming part of the original construction plans. A solar chimney consists of two parts: the solar collector (the section that heats up due to the absorption of solar energy) and the chimney section, which forms a channel for the airflow. The solar collector is positioned to the outside of the building to absorb solar energy. There is usually an opening at the bottom of the chimney into the house.

Air is heated inside the chimney and its density decreases. The inside house air however remains at a lower temperature and is subsequently more dense than the chimney air. The density difference between the chimney and the inside air causes movement of air from the region of higher density to lower density, meaning air from the inside room flows into the bottom of the chimney and forces the warmer air out into the atmosphere (see Figure 1.1). There is often a vent on the south side of the room which then allows cooler air to enter the building due to the chimney suction effect. If the air change rates are large enough, the room will be well ventilated.

Solar chimneys can also be used to ventilate and help cool down lofts and attics using the same concept. Since the vertical walls of an attic are not very high or in most cases non-existent, a solar chimney built at an incline as part of the roof must be used. The concept is exactly the same as a vertical chimney except that the chimney is of course positioned at the angle of the roof, and consequently the inclination angle will play a role in the air flow rate of the chimney as well as the exposed area for solar absorption. Again, solar chimneys used in roofs are mostly premeditated designs and require that parts of the roof be constructed of glass, which pushes up costs.

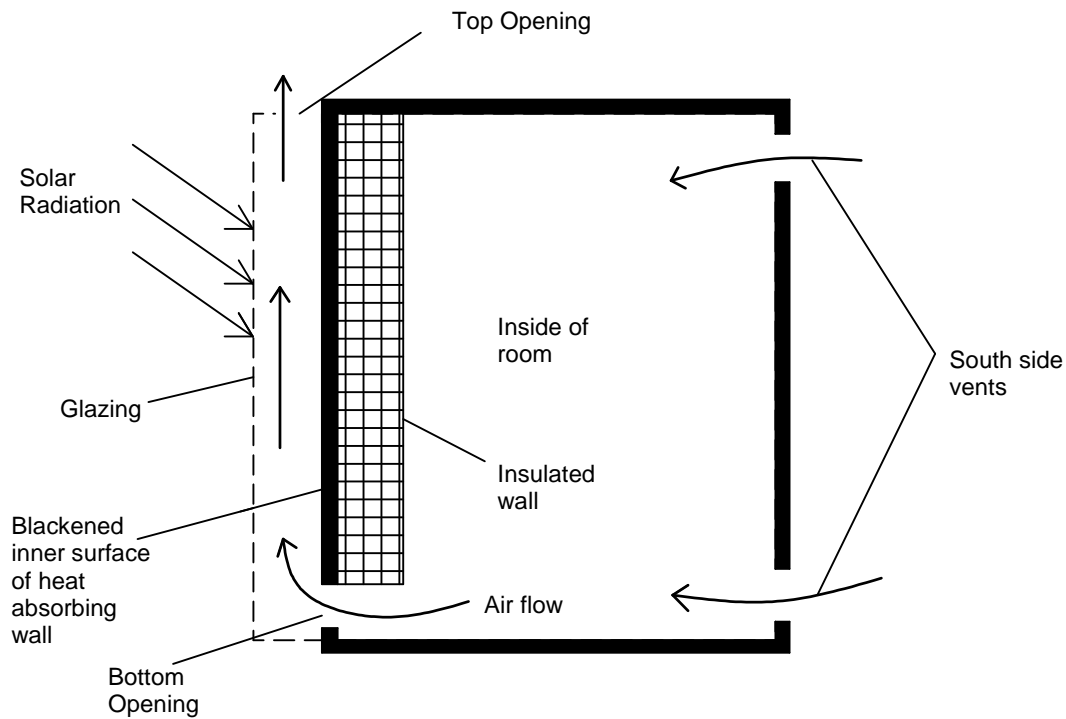


Figure 1.1: Solar chimney as part of the exterior wall of a building

Perhaps cost is part of the reason that passive systems have not been very popular especially in a developing country like South Africa. As seen above, passive thermal devices require expensive glazing and selective absorption coatings for increased thermal performance. However, if a cost effective system using cheaper materials could be designed, tested and found to be thermally effective, this will certainly have more appeal, especially to the poor, to satisfy their thermal comfort needs.

This report discusses the design and testing of such a thermal system; a *cost-effective* solar chimney built into and used to ventilate a loft for both summer and winter operation.

2 OBJECTIVES

A solar chimney constructed at an incline inside the corrugated iron roof of a loft will be tested with regards to enhancing natural air flow for cooling the loft in summer and recirculating warm air for heating in winter. The results will be compared to two other set-ups: a loft having only a single layer of roof insulation, for instance Isotherm™

(Brits, 2007), installed beneath the corrugated iron and one without any insulation, to determine the thermal effectiveness of the design and its suitability to South African climate conditions.

The design of the solar chimney will focus on simplicity and keeping costs at a minimum, hence it will differ from conventional chimney designs shown in Figure 2.1. The proposed chimney section consists of a corrugated iron roof, air gap, thermal insulation and ceiling board to create a channel for air flow, as shown in Figure 2.2. The design will use the sheet of corrugated iron as the solar collector as opposed to the glass and absorptive plate of usual designs.

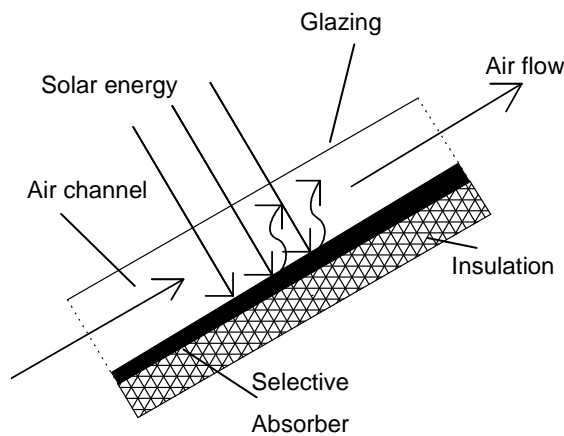


Figure 2.1: Sketch of conventional chimney design

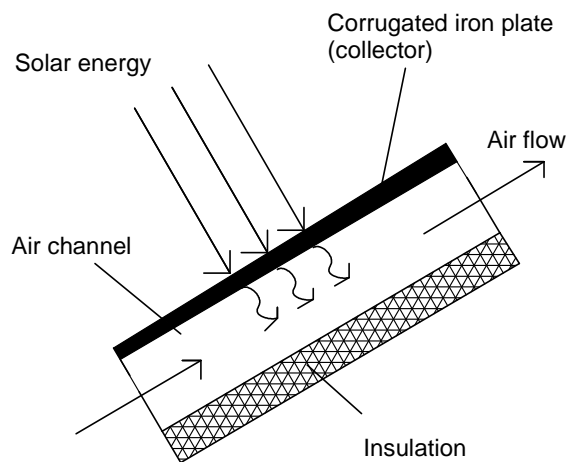


Figure 2.2: Sketch of proposed chimney design

The solar chimney enhances natural airflow through the loft in a similar manner as explained earlier for vertical chimneys (refer to Figure 2.3 below). In this design the sun's rays heat the corrugated iron, which in turn will transfer energy to the air in the channel of air causing the air to expand and decrease in density. The difference in densities between the chimney air and the loft space air will cause movement of air from the loft into the chimney, forcing the warmer air out of the chimney at the top. The warm air will either be released to the surrounding environment through a vent at the apex of the roof in summer, or, with the apex vent closed off, re-circulated into the loft during winter.

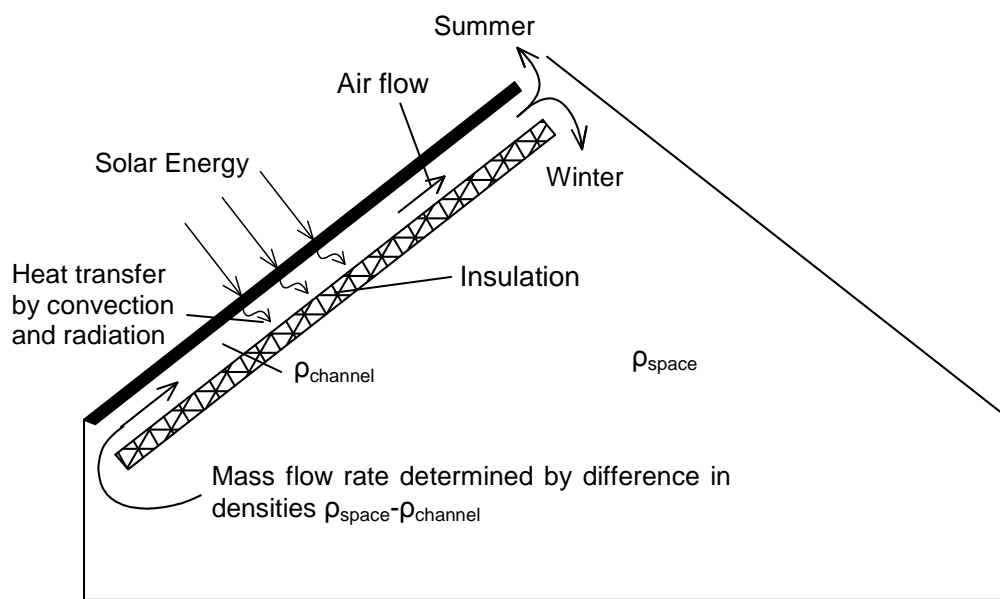


Figure 2.3: Principle of roof solar chimney concept

This project will focus on comparing the temperature readings obtained from the three separate compartments of the test-rig, where air temperature measurements will be taken from certain demarcated spots in the loft, and analytical results from a computer model simulation of the test-rig. One of the important things to determine is the overall effectiveness of the thermal system in comparison to the conventional design of Figure 2.1, and whether the design is an improvement to a roof with insulation but without a solar chimney.

The thermal effectiveness as stated here refers to the efficiency of the entire system, which, in the winter, since the aim is to heat the room up as much as possible, is the ratio between the amount of solar energy striking the corrugated roof over a period of time compared to how much of that energy is transferred to the air in the loft space, by the movement of air. This can be mathematically represented as,

$$\eta_{thermal} = \frac{mC_v\Delta T}{I_s A_r \zeta \Delta t} \quad (2.1)$$

where, m is the mass of the air in the room, C_v the specific heat (at constant volume) of the room air, ΔT the change in room air temperature from the start of the period of time to the end, I_s the incident solar radiation on a horizontal surface, A_r the roof's exposed collector area, ζ the geometric factor based on the inclination of the roof and the sun's declination and azimuth angles and Δt the time period that solar radiation falls on the roof.

For summer conditions, the solar chimney is required to enhance natural ventilation in the loft by increasing the temperature gradient between the air inside the chimney and the ambient air. The chimney in summer aims to increase the mass flow rate of fresh air and consequently the air exchange rate through the room. The system efficiency is then defined as the ratio of the amount of air exchanges experienced per hour in a room containing a solar chimney to that of a room without a chimney, otherwise known as a 'flow enhancing' efficiency. The 'efficiency' is in fact the percentage increase in mass flow rate from the room with no chimney to a room with a chimney. Mathematically the summer flow enhancing efficiency can be defined as,

$$\eta_{flow\ enhancing} = \frac{\dot{m}_{chimney} - \dot{m}_{no\ chimney}}{\dot{m}_{chimney}} \quad (2.2)$$

where, $\dot{m}_{no\ chimney}$ is the mass flow rate through a loft without a solar chimney and $\dot{m}_{chimney}$ the mass flow rate through an identical sized loft, assisted by the solar chimney concept.

A sensitivity analysis will also be conducted using the computer model to determine the effect of certain key variables of the system on its general performance. The results will be used to draw conclusions as to whether this is a feasible design for passive thermal applications and whether further design refinements are necessary.

3 LITERATURE REVIEW

Many designs, tests and models using the solar chimney effect for natural ventilation can be found in the literature. In the past decade, solar chimneys have attracted much attention in various investigations. These were mainly for summer operation in that the chimney was used to induce air changes and enhance natural ventilation in a building, while releasing warm air into the atmosphere.

Miyazaki *et al.* (2006) investigated the performance of a vertical solar chimney, using both CFD analyses and analytical means. Wall friction losses were not taken into account in their analytical model because the channel they investigated in the chimney was 1 m wide and thus frictional drag was regarded to play a negligible role in the momentum equation, which is actually never the case for natural ventilation in a passive system. It should be remembered however that an attic has limited space, and therefore a design using as little room as possible must be used while still ensuring noticeable air change rates. Wall friction must therefore be taken into account in an analytical model for a chimney in an attic, and could influence the rate of air changes substantially. The inclination angle of the solar chimney for a roof application will also have a definite influence on the air flow which was not taken into account for this vertical model. Nevertheless, the results obtained by Miyazaki *et al.* provide good information as to the development of these analytical models for solar chimneys in general.

Aboulnaga (1998), on the other hand, incorporates an inclined solar chimney in a roof and thus provides some valuable insight into the effects of the inclination angles on the performance of these chimneys. Unfortunately the chimney was built on the basis of the conventional chimney concept in that transparent glass and glazing were used

to obtain maximum heat transfer to the air from solar radiation. Their chimney is used to ventilate a room with a ceiling coupled with a wind cooled cavity to enhance air flow rates. The study found that the inclination of the solar collector played a significant role in the mass flow rates through the chimney and subsequently the rate of cooling of the room below. The optimum inclination angle for a *fixed* collector surface is such that it allows the maximum obtainable solar radiation absorption throughout the year regardless of the season, and is chiefly a function of the location latitude.

Another study performed by Hamdy *et al.* (1998) found that “both the average solar heat gain factor and the average intensity of solar radiation decrease as collector tilt angle increases. They have a maximum value for a horizontal collector while a minimum value for a vertical collector.” It is thus concluded that with regards to the tilt angle of a roof of a loft or attic which will be used for living in, the steeper the angle, the more living space available but the less efficient the performance of a solar chimney. This will have to be considered in the project.

Another factor influencing air flow rate is the rate of heat being transferred to the air in the chimney. This is directly proportional to the exposed area and the absorption coefficient of the solar collector. Bansal *et al.* (1993) analytically studied a solar chimney-assisted wind tower for natural ventilation in buildings. The authors developed an analytical model of a roof solar chimney by combining the energy balance equations of a conventional solar absorber with the air flow rate equations of chimneys. They found that for a room volume of 30 m³, an 30° inclined roof solar collector area of 2.25 m² and air channel height of 15 cm resulted in air exchange rates of between 4 and 6 per hour which is the required standard air change schedule for an office (Greenwood, undated). In conclusion the study observed that air flow rates are dependent on the geometry of the air collector, the size of the air duct of the channel and the performance parameters of the air heating solar collector. The estimated effect of the solar chimney was shown to be substantial in inducing natural ventilation for low wind speeds.

Kaneko *et al.* (2005) wrote a report on an inclined solar chimney with dimensions of 1.3 m length, 0.85 m width and channel depth of 0.2 m at an incline of 45° and found

airflow rates of 100 to 400 m³/h. This chimney was subject to a simulated solar radiation input in the shape of a sine curve over 9 hours with a maximum solar radiation of 1000 W/m². The chimney made use of the usual glass and coated aluminium plate as solar collector.

Another similar design to the one proposed for this study is found in a report by Hirunlabh *et al.*, 1999. Monier tiles and gypsum board, both common building materials, were used to form the air channel in the same manner as illustrated in Figure 2.2, with the tiles replacing the roof sheets and the gypsum board forming the lower insulation layer. Their design was validated using an analytical model in which the collector length and tilt angle were varied. In their report, the authors found that by increasing the length of the solar collector, increased the air flow rate, which is a consequence of the increased vertical height of the ventilation path. But the air flow rate *per unit area* decreased with increasing length of the collector. Thus, the amount of air flow rate induced by one longer collector would be lower than that induced by two shorter units of the collectors, with a total length equal to that of the longer unit. Thus it was found that to maximize the air ventilation by collector systems, the length of the collector should be shorter, in the order of 1 to 2 m. This length could be selected by architects, depending on the available surface area of roof.

For the roof tilt angle, an optimum combination must be found between the amount of solar radiation absorbed and the induced stack height of the chimney, i.e. the shallower the tilt angle, the more collector surface area is exposed to the sun and the more energy is absorbed and transferred to the air in the channel but the less the vertical height of the chimney. In their report, Hirunlabh *et al.*, 1999 found that for a latitude of 15° N, increasing the tilt angle up to 30°, the induced air flow rate increased rapidly due to the induced temperature difference. However, the vertical height is still too small to induce higher air flow rate, although the energy absorbed by the tiles was higher. For a tilt angle smaller than 60°, the increase of the air flow rate was found to be quite insignificant. Consequently, there is an optimum range of tilt angle based on latitude of location which for this report was found to be between 20 and 60°. They concluded further that such a design did not sufficiently induce natural ventilation to satisfy the resident's comfort, and that it should rather be incorporated with additional passive thermal devices.

As shown, there is ample literature regarding the testing and computer modelling of roof solar chimneys for summer operation which provide good insight and comparative data for this proposed chimney design for summer conditions. But there is in general a lack of information regarding the use of solar chimneys for a winter application as explained earlier for heating a roof space, and very little information on the use of common building materials used for construction or at least a comparison between cost-effective designs for the collector itself.

4 EXPERIMENTAL WORK

4.1 Design and construction of test-rig

Design

The proposed test rig represents a half-scale model of a typical loft as shown in Figure 4.1, with the dimensions given in meters. Referring to Figure 4.1, the structure consists of a wooden frame to support the 45° inclined corrugated iron roof, 100 mm thick polystyrene board 'floor' and 50 mm thick polystyrene board exterior walls. Regarding the choice of the roof tilt angle, it is generally accepted that the optimum angle for a fixed solar collector to obtain a maximum amount of solar radiation averaged over a year, is the degree of latitude of the specific location. The latitude of the testing facility is 34.2° S, but to make the roof inclination angle equal to this would mean there would be very little space inside the loft for people to live in. Hence, the inclination of the roof angle was decided upfront to be 45° to increase the available volume of the loft.

The loft space was further divided into three separate 'compartments' or sections for the three different experiments discussed earlier (solar chimney, bare roof, roof with insulation). The partitions separating the three sections will consist of 25 mm thick polystyrene board to thermally isolate the three sections from one another. In doing this, accurate comparative results will be obtained between the three compartments without the need to build three completely separate structures.

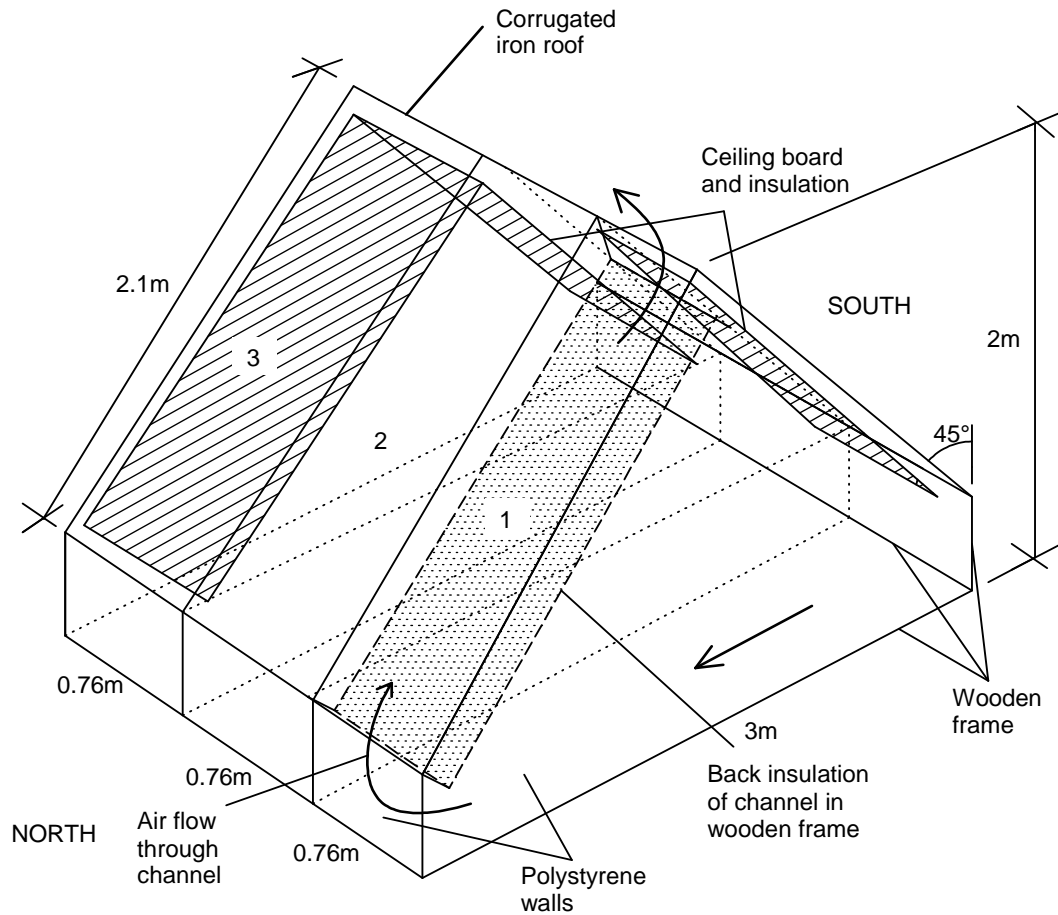


Figure 4.1: Proposed test-rig showing three separate compartments

Compartment one contains the solar chimney which was constructed from a wooden frame nailed to the underside of the roof's supporting trusses. The frame provides the gap for the airflow and support for the chimney's lower section, consisting of a layer of Isotherm™ insulation and ceiling board, as shown in Figure 4.2.

Referring back to Figure 4.1, compartment two contains a bare corrugated roof, in effect providing a control for the experiment. In addition, seeing that many lower income houses in South Africa often have nothing else other than a bare corrugated iron roof, this compartment will also provide readings for these comparative purposes.

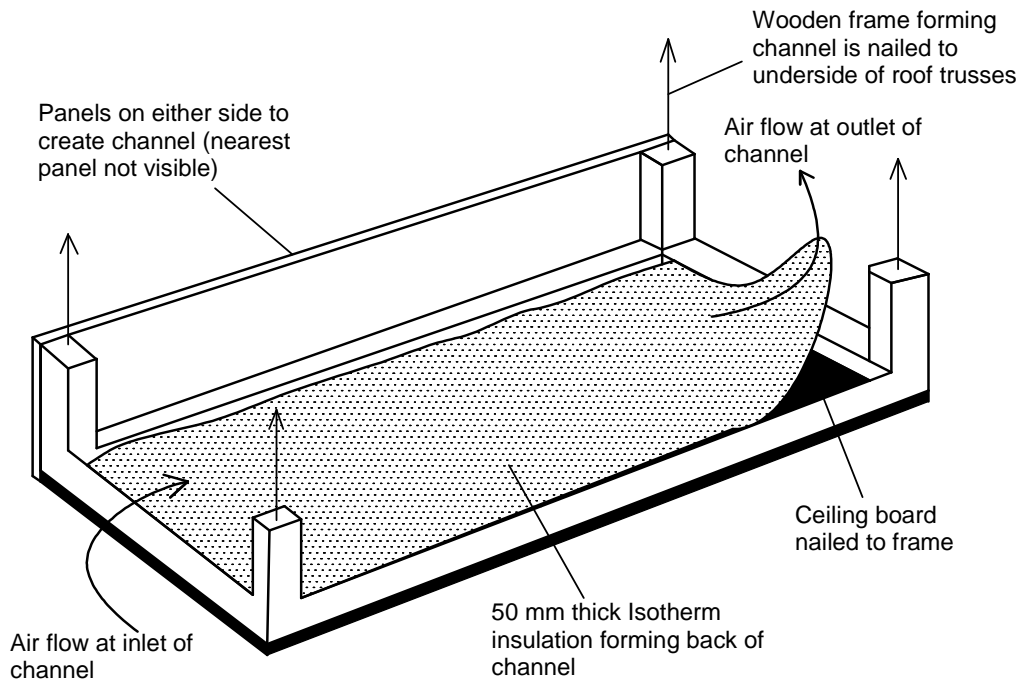


Figure 4.2: Construction of the solar chimney's lower section

Compartment three will contain a layer of Isotherm™ (Brits, 2007) roof insulation between the corrugated roof and a panel of ceiling board. This is to simulate the usual roof insulation installed below the roof surfaces of most houses. The aim is to determine whether the compartment containing the solar chimney will see more satisfactory results compared to this compartment, and subsequently the feasibility of installing a solar chimney for enhanced thermal comfort in addition to roof insulation.

Building materials

In addition to polystyrene board, wooden beams and corrugated iron roofing sheets, other materials included in the construction were:

- Hardboard for support of polystyrene board
- Ceiling board (6 mm thick)
- Isotherm™ (Brits, 2007) roof insulation (50 mm thick)
- Silicone glue, duct tape, screws and nails
- Concrete weights to secure the entire structure to the ground

The ceiling board was used to secure the Isotherm™ insulation (Brits, 2007) against the inner roof surface of the South facing side of the roof in the chimney compartment, and for both the North and South facing sides in the third compartment as shown in Figure 4.1 and 4.2.

Site

The test-rig was erected outside on top of one of the Mechanical Engineering Department building roofs ('solar testing facility'), where maximum, uninterrupted solar radiation would prevail. The latitude of the location as mentioned previously is 34.2° S. The structure was further orientated in a North-South direction such that the inclined roof containing the chimney faced true North, to capture the optimum amount of solar energy for southern hemisphere conditions. A photo of the test-rig in winter operation i.e. with the apex vent closed, is shown in Figure 4.3.

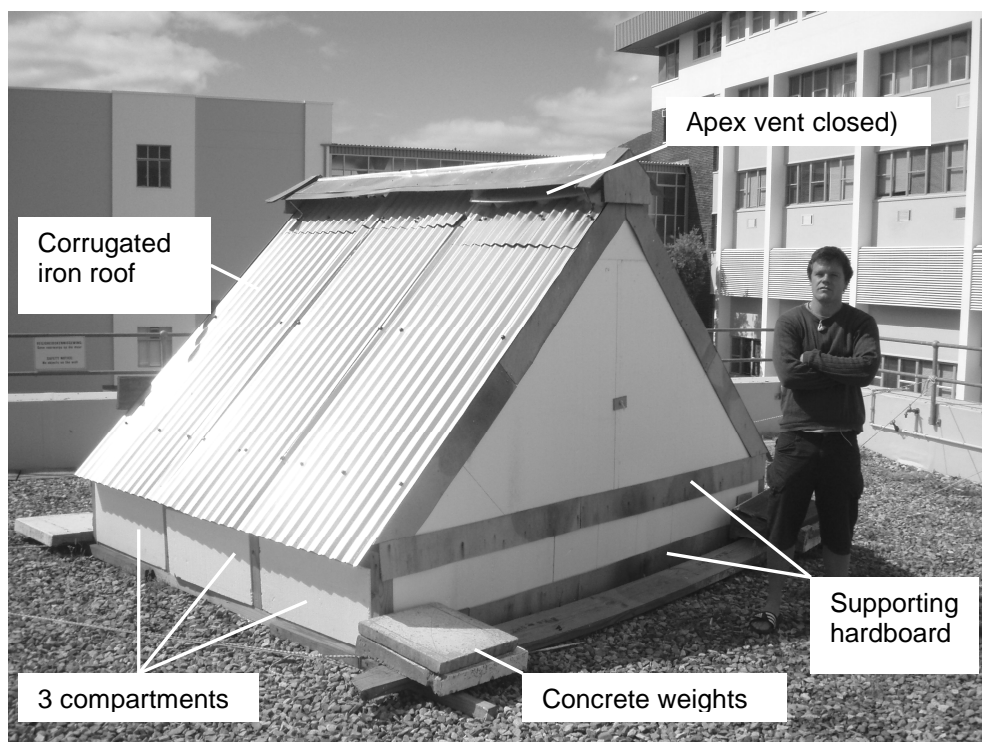


Figure 4.3: Test-rig built on site

4.2 Operation

Experiments were conducted in June and November concentrating on winter and summer conditions respectively. The aim of the experiments was to identify temperature changes and trends inside the compartments and the differences between summer and winter operation.

4.2.1 Summer conditions

During the summer months, the solar chimney compartment test rig is expected to produce the air flow patterns as illustrated in Figure 4.4, to keep the compartment cool and well ventilated. Two vents are present in the figure; one at the south wall at the bottom to allow cooler air to enter, and one at the apex of the roof to allow the hot air from the chimney to escape. This ensures a continuous replacement and ventilation of air in the compartment.

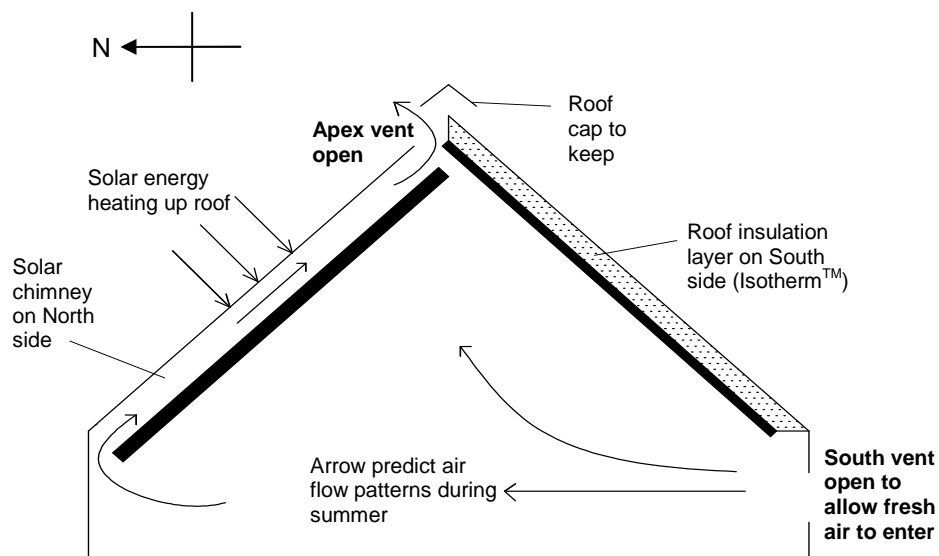


Figure 4.4: Expected operation of test-rig during summer

4.2.2 Winter conditions

During the winter months adjustments were made to the solar chimney compartment such that the entire compartment was sealed. The apex vent and south wall vent were

closed to keep the warm air re-circulating through the compartment. This is illustrated in Figure 4.5.

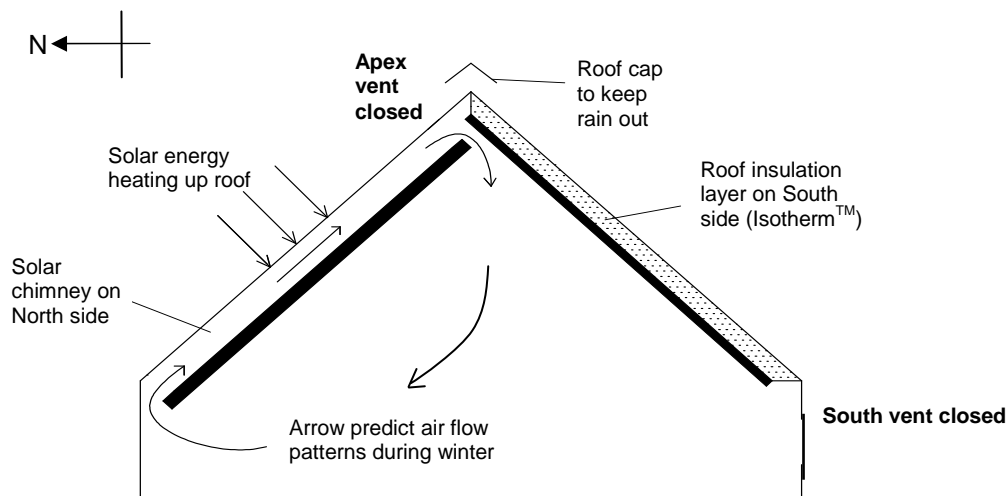


Figure 4.5: Expected operation of test-rig during winter

4.3 Instrumentation

The room air temperature of all three compartments was measured at three levels using T-type thermocouples with an accuracy of $\pm 0.2^{\circ}\text{C}$, positioned in the middle of each room, 0.2 m, 1.2 m (mid-height) and 2.2 m above ground level respectively. The thermocouple at the top in the chimney compartment in effect measured the outlet temperature of the chimney and in addition another thermocouple was positioned at the chimney inlet to determine if the air did in fact experience a temperature increase through the chimney as expected. The positions of all 11 sensors are shown in Figure 4.6, where the sketch on the left shows a view from the west with the solar chimney compartment in the front, and the sketch on the right shows a view from the north.

The data logger used to process the sensor measurements was a Schlumberger SI 35951A IMP model, with input connector manufactured by Solartron Instruments. Measurements were taken every second, while data was stored every 5 minutes in order to get an accurate graph for an average two day period. The data was stored and further processed on a computer in a neighboring laboratory.

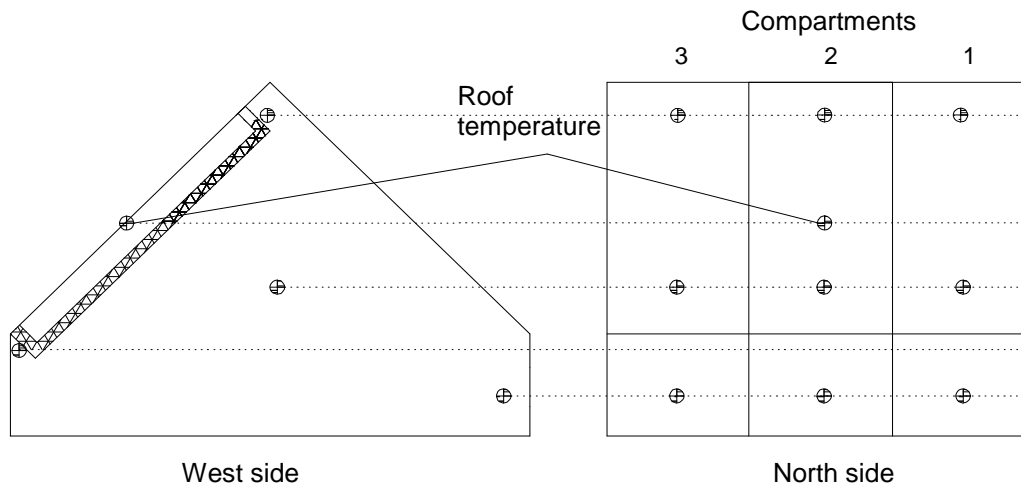


Figure 4.6: Placement of temperature sensors in the test-rig

In addition to the test-rig instrumentation, a weather station was set up near the test rig to obtain readings of the wind speed and direction, ambient indoor and outdoor temperatures and solar radiation during the testing period. Figure 4.7 shows a photo of the weather station. The data was captured using an anemometer, shielded temperature sensor and solar radiation sensor from Davis weather station instrument suppliers and a Davis Energy EnviroMonitor® data logger (Davis Instruments Corp., 2007). Measurements were stored every half hour and saved to the computer to be used for referencing and data interpretation.

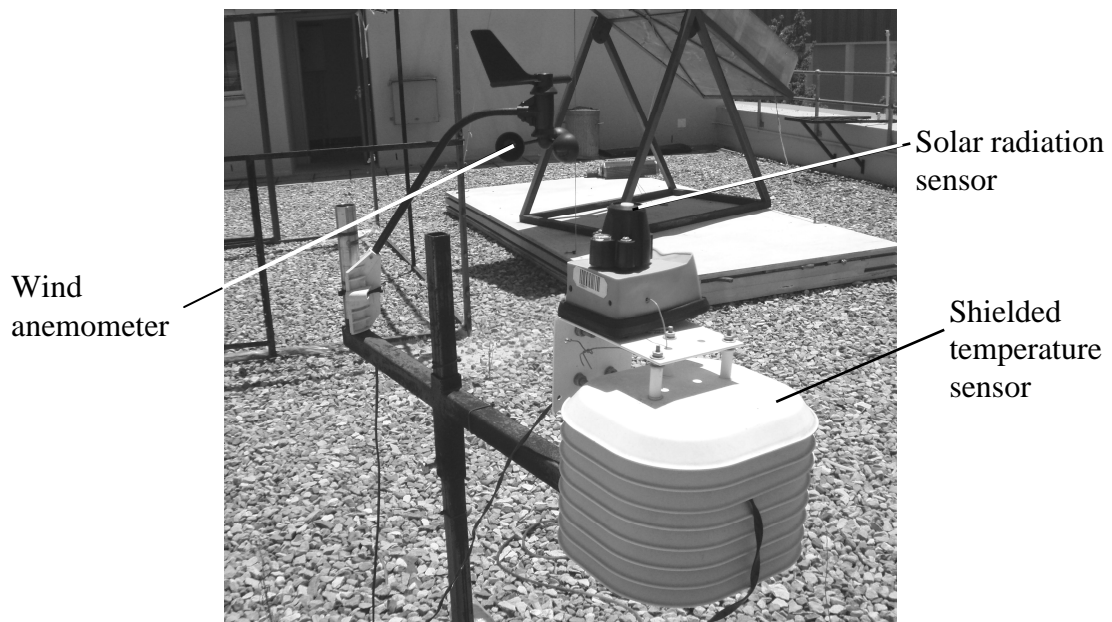


Figure 4.7: Weather station set up near test-rig

4.4 Results

Large amounts of raw data were captured on a daily basis using the instrumentation above. It was decided to only plot and display each compartment's average room temperature, the overall roof temperature and the ambient temperature against time since the aim of the experiment is to compare results on the overall thermal effect between the three set-ups and against ambient conditions. The roof temperature is very sensitive to cloud cover and the effect clouds have on the solar radiation falling on the corrugated roof as will be indicated in the graphs. The incident solar radiation measured by the radiation sensor is plotted on the secondary y-axis.

4.4.1 Winter operation

The results for two typical sunny (cloudless) days in winter are shown in the following graph (Figure 4.8). The first thing to notice is that the roof temperature is very sensitive to ambient conditions which results in the constantly varying curve. The ambient air reaches a maximum of 18 °C on the first day and 22 °C on the second day. All three room temperatures are above the ambient temperature while the sun is shining on both days and remain so into the evening and night of the first day.

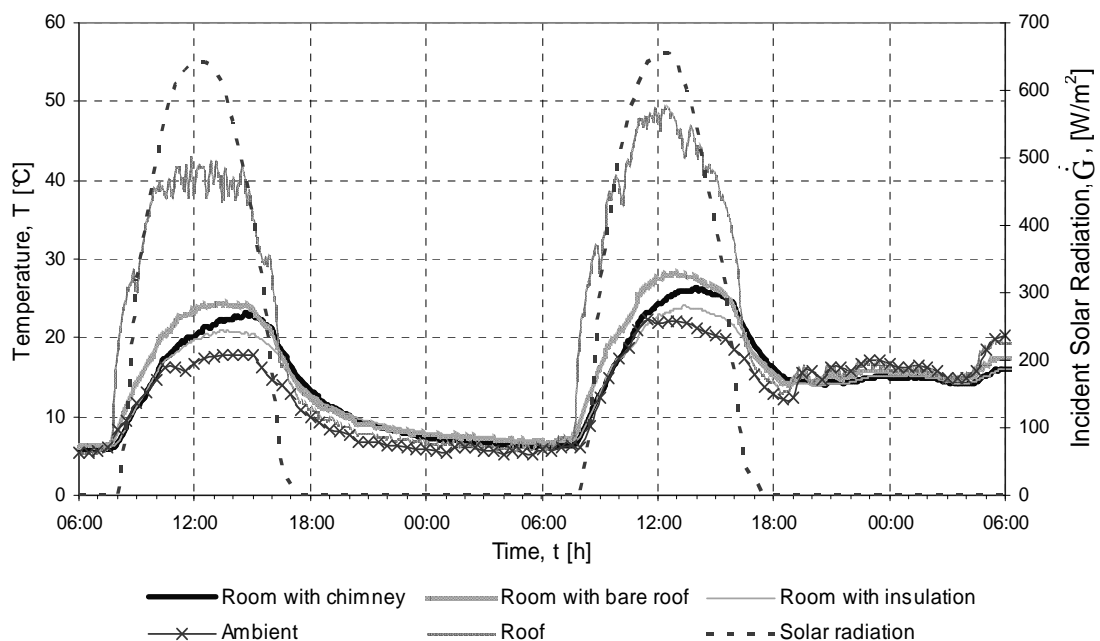


Figure 4.8: Two typical sunny days in winter

Naturally, the room with the bare corrugated roof heats up the most during the day but also cools down faster than the room with the chimney or insulation. Both these rooms have a slight time lag due to the increased heat capacity of the additional building materials, and thus heat up and cool down about an hour later than the room with the bare roof.

On both days one notices that the room with the solar chimney is slightly warmer (by 2-3 °C) than the room with roof insulation and the chimney room is also 5 °C higher than ambient temperature at the 10th hour, corresponding to 16:00 in the afternoon. These are not large differences but nonetheless prove that the solar chimney warms the loft space to some extent. At night however, one notices that the chimney room has the lowest temperature, this being because the solar chimney is in fact working in reverse as the night ambient temperature cools the roof and subsequently the air in the chimney. It was seen that the room actually becomes cold more quickly than the other two rooms because of the chimney concept acting in reverse, otherwise known as “reverse thermosyphoning”. In future, air must be prevented from sinking down from the cold chimney channel at nights to stop this from occurring.

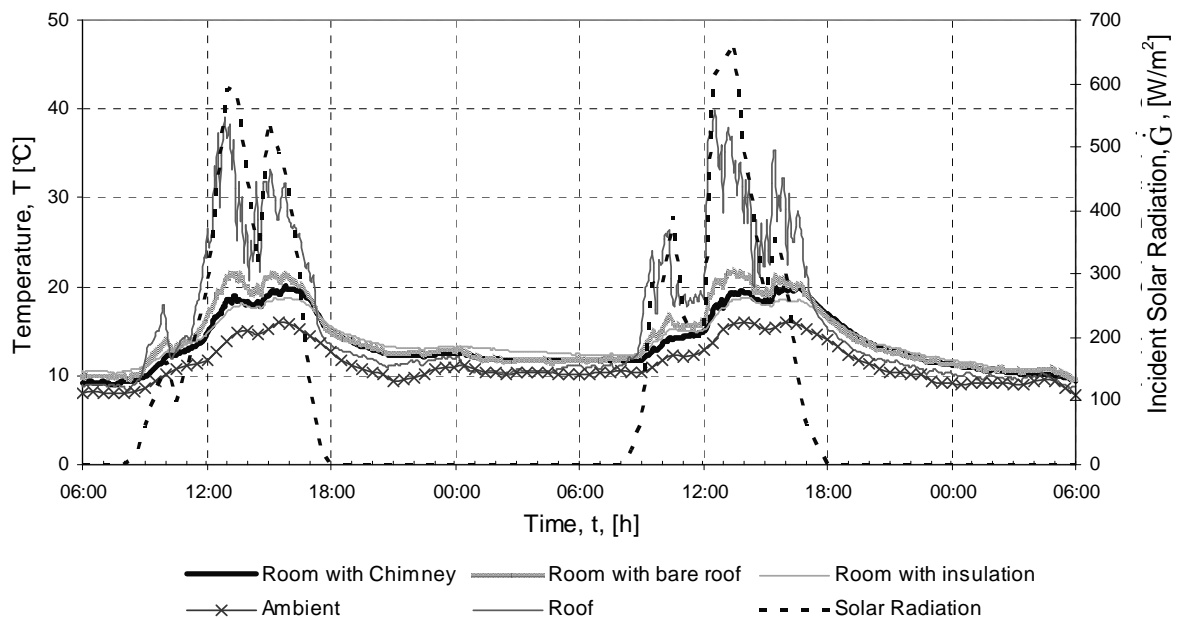


Figure 4.9: Two typical cloudy days in winter

The above graph (Figure 4.9) shows two typical cloudy days in winter and clearly shows the effect that clouds have on firstly the amount of incident solar radiation striking the roof and secondly the smaller differences between day and night temperatures and the higher ambient temperatures during the night due to the cloud 'blanket' effect. Because less solar radiation is being absorbed by the solar chimney collector, the room with the chimney does not function as well as it did for a clear day and hence it is practically the same temperature as the room with insulation. All three rooms however, are able to retain a higher temperature (3-5 °C) than ambient for most of the day while the sun shines but all temperatures drop to being nearly equal during the night. The room with the insulation performs the best at night when it is able to trap some of the heat transferred during the day. The cloudy conditions show that the solar chimney does not function efficiently when there is insufficient solar radiation, which is to be expected.

4.4.2 Summer operation

Unfortunately the weather was not ideal for summer operation as the ambient temperatures for most of the month of November were not very high. It should be noted that the experiments should ideally be conducted during the hottest months of the year for summer operation which, for the specific location in question, will be January or February. The results for two typical days in November, i.e. summer operation are plotted below in Figure 4.10.

Referring to Figure 4.10, the first day was a clear day indicated by the smooth curve for the incident solar radiation on a horizontal plate as measured by the solar radiation sensor. The second day was slightly cloudy and is reflected by the less smooth solar radiation curve. As expected, the room with no insulation and no solar chimney, with just a bare corrugated roof experienced the highest temperatures during both days. On the first day, the room with the insulation experienced slightly higher temperatures (3 °C higher) than the room with the chimney, which closely matched the ambient temperatures throughout the two days. On the second day it is clear that both the insulated room and the room with the solar chimney experience very similar temperatures and both follow the ambient temperature.

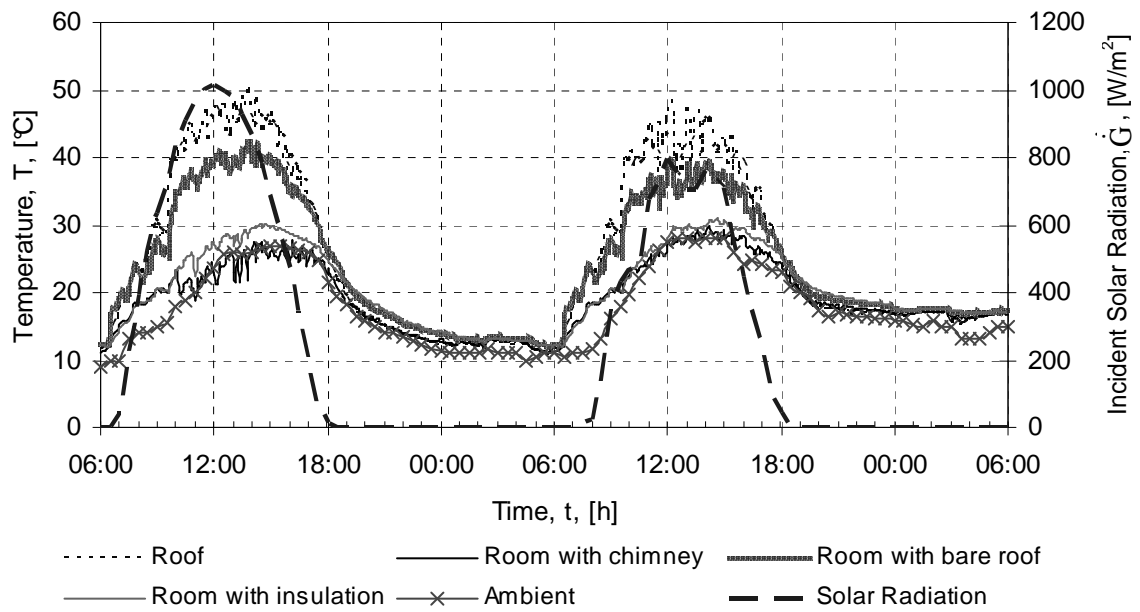


Figure 4.10: Two typical days in summer

As no mass flow rate experiments were conducted due to time constraints, it was difficult to evaluate the solar chimney's performance against the other two rooms, although it can be concluded that the solar chimney maintains the room air at ambient conditions as expected. The real value of a solar chimney during summer is measured by its flow enhancing efficiency as defined in Chapter 2. Since no mass flow rates through the room were measured during the experimental procedure, they were calculated analytical using a computer simulation model of the test-rig as which will be discussed in the analytical study.

5 ANALYTICAL STUDY

5.1 Thermal model

The major objectives of the analytical study were to predict the air flow rates through the chimney and loft, provide results which could be compared to the experimental data obtained and study the effect of changing certain variables of the system on the

performance of the solar chimney. For the thermal analysis the following assumptions were made:

1. there is a one-dimensional heat flow through the solar collector (corrugated roof) as well as through loft wall insulation (polystyrene)
2. the heat capacity of all solid materials are considered, thus heat transfer is under unsteady state conditions
3. the effect of corrugation of the roof is neglected, hence the cross-section of the air channel is assumed to be rectangular and shading due to the corrugations is negligible
4. properties of air are functions of temperature
5. the sky can be considered as a black body for long wavelength radiation at an equivalent sky temperature
6. air leakage effect is negligible
7. properties of materials are temperature independent
8. dust and dirt on the collector roof are negligible

5.1.1 Winter

The thermal model is presented with the aid of Figure 5.1 in which the most important components, variables and parameters of the system are shown. Although the room or space of the test-rig has a complicated shape, the model here represents the room as a large tank in which thorough mixing of the air occurs.

Sunlight energy is absorbed by the roof, which heats up and subsequently transfers heat to the air in the air channel formed between the roof and the insulation. The roof and air channel are divided up into control volumes depicted by $i-1$, i , $i+1$, etc. as seen in the figure. The Section A-A in the figure shows a cross section of such a control volume.

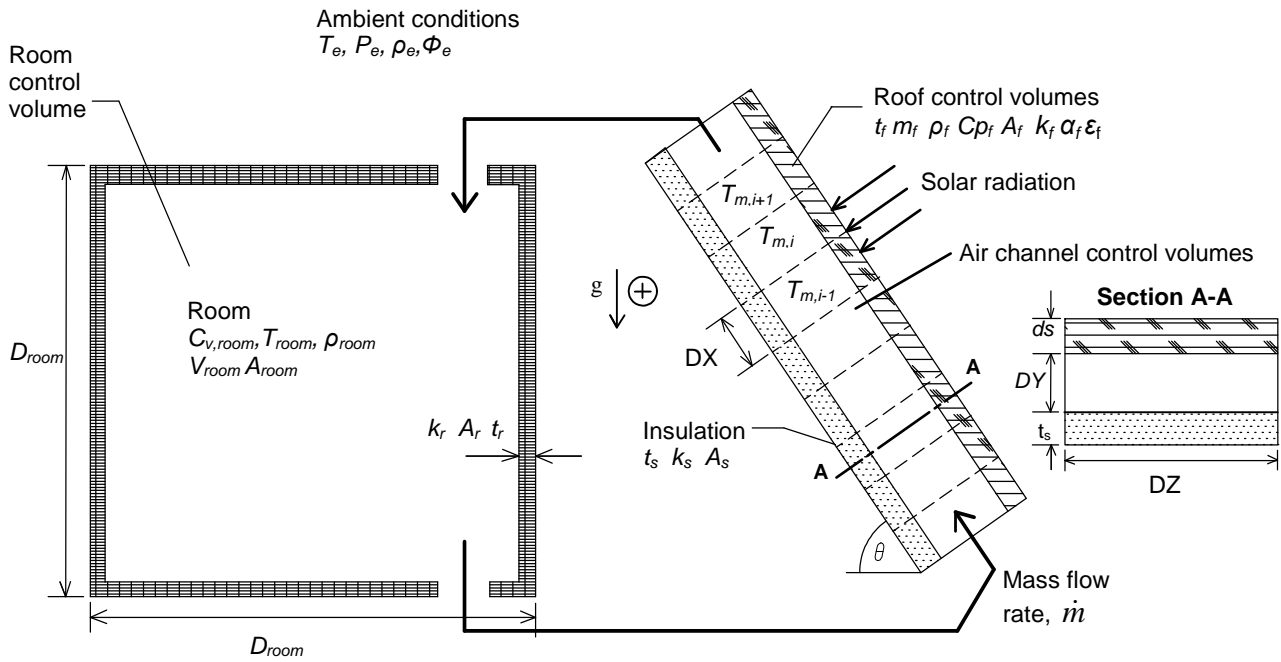


Figure 5.1: Most important parameters of winter analytical model

The air in the channel heats up and the density decreases. The room air is initially at a lower temperature and higher density than the channel air. This density gradient causes the downward movement of air from the room and upwards through the channel as indicated by the arrows, i.e. the solar chimney driving force. The room heats up accordingly, and loses heat to the surrounding environment at ambient conditions through the walls of the room. The roof loses heat by natural convection and radiation to the environment. Some of the heat reaches the room air via the back half of the air channel through the layer of insulation. Gravity is depicted by the constant gravitational acceleration g and its direction is depicted as positive in the downward direction.

Conservation of mass

Considering the mass flow rate throughout the system remains constant at a given time step and is a function of the velocity v , density of the fluid in motion ρ and the cross-sectional area A_c as follows:

$$\dot{m} = \rho v A_c \quad (5.1)$$

Conservation of energy applied to the roof

Thermally the roof can be considered as a radiation panel, absorbing solar energy to be transferred to the air in the channel. The roof is divided up into 9 control volumes along its length as shown in Figure 5.1. These control volumes coincide with the control volumes of the channel. The roof is simplified to have negligible thermal mass because its thickness, ds , is only $= 0.6$ mm. The roof absorbs a portion of incident solar energy according to a view and geometric factor ζ (defined in Appendix B.1) as well as the absorptivity α_f of the specific roof material. The roof radiates energy to the surrounding sky according to the sky temperature T_{sky} and also loses energy via natural convection subject to the ambient air temperature T_e and the natural convection coefficient h_{up} . The convection coefficient is a function of the Reynolds number (indicating laminar or turbulent flow) depending on the wind velocity profile given in Figure B.6, as well as the density of the ambient air ρ_e , angle of the roof θ and roof length DX . Further, the roof transfers heat to the air in the channel at a temperature of T_m , with a heat transfer coefficient h_{down} . This heat transfer coefficient is defined similar to h_{up} with the Reynolds number being determined by the velocity of the airflow in the channel. It was assumed that negligible energy flowed from one control volume of the roof to the next due to conduction.

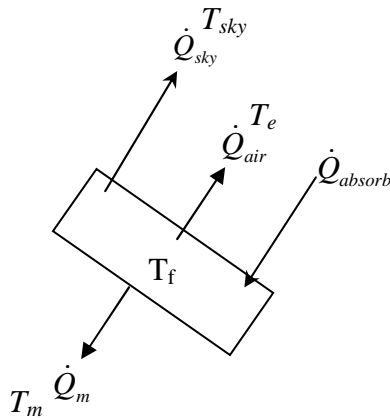


Figure 5.2: Control volume for roof section

By referring to Figure 5.2, the heat transfer equations can be written as follows:

The radiation heat transfer rate from the roof to the sky is:

$$\dot{Q}_{sky} = \varepsilon_f \sigma A_f (T_f^4 - T_{sky}^4) \quad (5.2)$$

where $T_{sky} = \left[\varepsilon_{sky} (T_e + 273.15)^4 \right]^{1/4} - 273.15$, $\varepsilon_{sky} = 0.741 + 0.00162T_{dp}$ at night time and $\varepsilon_{sky} = 0.727 + 0.00160T_{dp}$ during the day (Mills, 2000).

Using the Magnus-Tetens formula (Barenburg, 1974) for the dew point temperature:

$$\text{where } f = \frac{aT_e}{(b + T_e)} + \log(\phi)$$

$$a = 17.27$$

$$b = 237.7$$

and ϕ is the relative humidity (Barenburg, 1974)

The convective heat transfer rate to the environment is:

$$\dot{Q}_m = h_{up} A_f (T_f - T_e) \quad (5.3)$$

where $h_{up} = f(\text{Re}_f, \theta_f, T_f, T_e, DX_f, \rho_e)$. Refer to Appendix A for the calculation of the convection heat transfer coefficient.

The convective heat transfer rate from the roof to the air in the channel control volume is similarly:

$$\dot{Q}_{air} = h_{down} A_f (T_f - T_m) \quad (5.4)$$

where $h_{down} = f(\text{Re}_m, \theta_f, T_f, T_m, DX_f, \rho_m)$. Refer to Appendix A for the calculation of the convection heat transfer coefficient.

For the solar radiation being absorbed by the roof:

$$\dot{Q}_{abs} = \zeta_{winter} \alpha_f A_f \dot{G}_{winter} \quad (5.5)$$

Where ζ_{winter} represents a constant determined by the position of the sun in the sky, the latitude of the location and the inclination and orientation angle of the roof, α_f is the absorptivity of the roof, A_f the exposed area of one control volume of the roof and

\dot{G}_{winter} is the incident solar radiation as described by the input graphs of Figure B.1 and Figure B.3 in Appendix B.1 and based on average solar intensity for the month of June. The solar radiation geometric factor ζ_{winter} is also calculated and plotted in Appendix B.1.

The change in temperature of the roof over a given amount of time $\Delta t = t_2 - t_1$ is then given by:

$$T_f^{t_2} - T_f^{t_1} = \frac{(\dot{Q}_{\text{absorb}} - \dot{Q}_{\text{sky}} - \dot{Q}_{\text{air}} - \dot{Q}_m)}{m_f C} \Delta t \quad (5.6)$$

where m_f is the mass of the roof control volume and is simply:

$$m_f = (\rho_f)(DY)(DX)(ds)$$

and C = specific heat of roof material.

Conservation of energy applied to the air channel

The air channel is divided into 9 control volumes along its length as shown in Figure 5.3 corresponding to the control volumes of the roof as mentioned before. Air flows through the channel absorbing heat \dot{Q}_{convec} from the hot roof and transfers it to the room. Some heat transfer \dot{Q}_{conduc} also occurs through the back side of the channel into the room through the insulation layer. Energy is also carried in and out of the control volume by mass transfer in the form of enthalpy h . One control volume, i , of the air channel is shown in Figure 5.3.

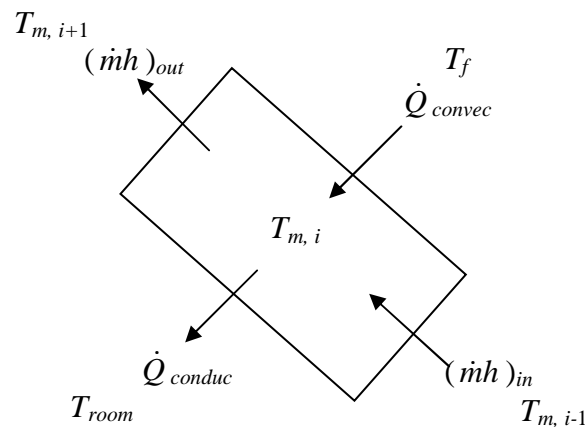


Figure 5.3: Sketch of air channel control volume

The convective heat transfer from the hot roof to the air in the channel is:

$$\dot{Q}_{convec} = h_{down} A_f (T_f - T_{m,i}) \quad (5.7)$$

and is similar to \dot{Q}_m from the roof section discussed above.

The conductive heat transfer from the air in the channel to the inside of the room through the layer of insulation is:

$$\dot{Q}_{conduc} = \frac{k_s A_s (T_{m,i} - T_{room})}{t_s} \quad (5.8)$$

where k_s is the thermal conductivity of the insulation material, A_s the heat transfer surface area, and t_s the thickness of the insulation.

Energy is brought into and out of the control volume by the movement of air, the mass flow rate \dot{m} through the channel. Energy transferred into the control volume is:

$$\dot{Q}_{in} = (\dot{m}h)_{in} \quad (5.9)$$

where $h = C_p T_{m,i-1}$ is the enthalpy term, C_p is the specific heat of the air, and the $T_{m,i-1}$ is the temperature of the previous control volume. Similarly, energy being transferred via mass flow out of the control volume is:

$$\dot{Q}_{out} = (\dot{m}h)_{out} \quad (5.10)$$

where $h = C_p T_{m,i}$.

Finally the change in temperature of the control volume over a given amount of time $\Delta t = t_2 - t_1$ is then:

$$T_m^{t_2} - T_m^{t_1} = \frac{\dot{Q}_{convec} + \dot{Q}_{in} - \dot{Q}_{conduc} - \dot{Q}_{out}}{m_m C_v} \Delta t \quad (5.11)$$

where m_m is the mass of the air in the control volume and C_v the specific heat.

Conservation of energy as applied to the room

The room is treated as one control volume and it is assumed that thorough mixing of the air occurs within the space, i.e. the temperature of the room is uniform. The room dimensions are arbitrarily chosen such that its height equals its diameter thus making it possible to express its surface area and volume in terms of only one variable, its diameter D_r . The room receives or loses heat via mass transfer from the channel as

well as via conduction through the room walls to the environment and to the air in the chimney. The room control volume is sketched in Figure 5.4 as follows:

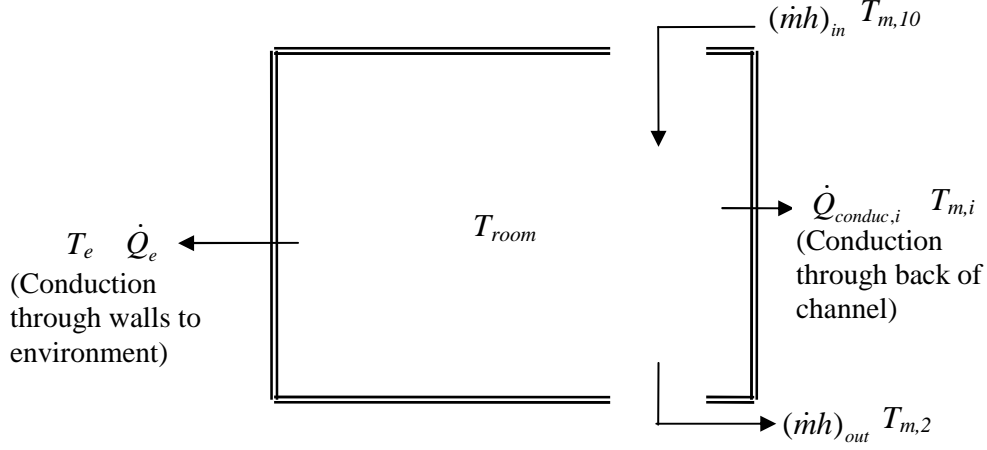


Figure 5.4: Sketch of room control volume

Heat transfer via conduction to the channel through the insulation at the underside of the channel is:

$$\begin{aligned}\dot{Q}_{conduc} &= \sum_{i=2}^{10} \dot{Q}_{conduc,i} \\ &= \frac{k_s A_s (T_{room} - T_{m,i})}{t_s}\end{aligned}\quad (5.12)$$

Heat transfer to the environment through the walls of the room is:

$$\dot{Q}_e = \frac{k_{room} A_{room} (T_{room} - T_e)}{t_r}\quad (5.13)$$

where A_{room} is the total exposed area of the room to the environment and is $A_{room} = D^2/4 + \pi D^2$, k_{room} is the thermal conductivity of the wall material and has the same value as k_s and t_r is the thickness of the wall.

Energy is brought into and out of the room by the movement of air, the mass flow rate \dot{m} into and out of the channel. Energy brought into the room is:

$$\dot{Q}_{in} = (\dot{m} h)_{in}\quad (5.14)$$

where $h = C_p T_{m,10}$ is the enthalpy term, C_p is the specific heat of the air, and $T_{m,10}$ the temperature of the last channel control volume. Similarly, energy being transferred by mass out of the room is:

$$\dot{Q}_{out} = (\dot{m}h)_{out} \quad (5.15)$$

where $h = C_p T_{room}$.

Finally the change in temperature of the room over a given amount of time $\Delta t = t_2 - t_1$ is then:

$$T_{room}^{t_2} - T_{room}^{t_1} = \frac{\dot{Q}_{convec} + \dot{Q}_{in} - \dot{Q}_e - \dot{Q}_{out}}{m_{room} C_v} \Delta t \quad (5.16)$$

where m_{room} is the mass of the air in the room control volume and C_v the specific heat.

Conservation of momentum

The conservation of momentum is applied to one control volume of the air in the channel and room as shown in Figure 5.5:

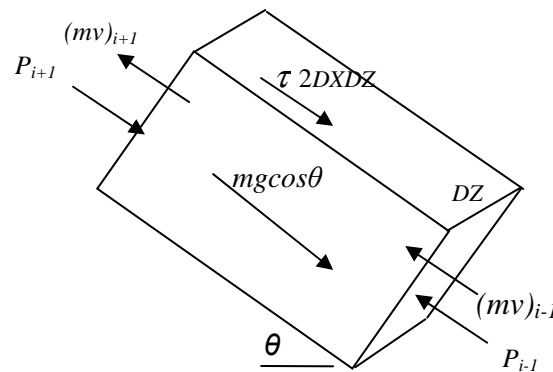


Figure 5.5: Law of momentum applied to one control volume

The equation of the law of momentum applied to this control volume may be written as:

$$\frac{\Delta(mv)}{\Delta t} = (\dot{m}v)_{i+1} - (\dot{m}v)_{i-1} - (P_{i+1} - P_{i-1})A_c + mg \cos \theta - 2\tau DXDZ \quad [N]$$

or

$$\frac{\Delta(mv)}{\Delta t} = (\rho A_c v^2)_{i+1} - (\rho A_c v^2)_{i-1} - (P_{i+1} - P_{i-1})A_c + \rho DX A_c g \cos \theta - \frac{C_f \rho v^2 2DXDZ}{2} \quad (5.17)$$

Regarding the channel only, the equation is divided by the cross sectional area A_c of the channel and all the momentum terms for each control volume are added together. The Boussinesq approximation was assumed in that the density is considered constant except in the buoyancy term (the first term on the right hand side of the equation):

$$\frac{\Delta v}{\Delta t} = \frac{\sum_{i=2}^N (\rho DX g \sin \theta)_i}{\sum_{i=2}^N (\bar{\rho} DX)_i} - \frac{(P_{N+1} - P_0)}{\sum_{i=2}^N (\bar{\rho} DX)_i} - \frac{\sum_{i=2}^N \left(\frac{C_f \bar{\rho} v^2 2DXDZ}{2A_c} \right)_i}{\sum_{i=2}^N (\bar{\rho} DX)_i} \quad (5.18)$$

In the second term, P_{N+1} and P_0 are the pressure terms and depend on the room temperature. The pressure terms are calculated according to the temperature and density of the room air as $P_{N+1} - P_0 = \rho g h_{room}$, where $\rho = \rho$ at T_{room} , and h_{room} is the vertical height of the room (and chimney).

The third term represents the losses due to friction of the air along the walls and bends of the channel. These losses are taken into account by the addition of an appropriate equivalent length L_{equ} to DX representing the expansion and contraction losses as the air enters and exits the channel. For an expansion of the channel into the room the equivalent length is $L_{equ} = 35D_{hyd}$, and for contraction from the room into the channel, $L_{equ} = 16D_{hyd}$ (Batty *et al.* 1983), where the hydraulic diameter D_{hyd} of the channel is:

$$D_{hyd} = \frac{4A_c}{2(DY + DZ)} \quad (5.19)$$

The friction factor C_f is calculated according to the characteristics of the flow through the channel represented by the Reynold's number. The Reynold's number is dependent on the velocity v , density ρ and dynamic viscosity μ of the flow over a

certain channel length. These variables and the Reynolds number are calculated in Appendix A. The friction factor is then defined as $C_f = 1$ if the Reynolds number is below 16, $C_f = 16/\text{Re}$ if the Reynolds number is between 16 and 1181, otherwise $C_f = 0.078\text{Re}^{-0.25}$. The final equation is then:

$$\frac{\Delta v}{\Delta t} = \frac{\sum_{i=2}^N (\rho DX g \sin \theta)_i}{\sum_{i=2}^N (\bar{\rho} DX)_i} - \frac{(P_{N+1} - P_0)}{\sum_{i=2}^N (\bar{\rho} DX)_i} - \frac{\sum_{i=2}^N \left(\frac{C_{fi} \bar{\rho} v^2 2(DX + L_{eq}) DZ}{2A_c} \right)_i}{\sum_{i=2}^N (\bar{\rho} DX)_i} \quad (5.20)$$

In essence, the above equation illustrates that the velocity of the air flowing through the channel depends on three terms. Firstly, the driving term depending on the density of the air in the channel, which depends essentially on the temperatures calculated for the air in the channel. A second term retarding the driving force due to the room conditions being different to that of the channel (if the room were to be cooler than the channel, the air would be more dense and the retarding term would be greater in magnitude than the buoyancy term, causing air to flow at a certain velocity up through the channel). Thirdly, the last term represents frictional losses and depends essentially on the velocity of the air. By solving for the momentum equation through the natural circulation loop for a set value of temperatures, the air flow velocity at a certain cross-sectional area can be calculated and consequently the mass flow rate of the system.

5.1.2 Summer

The thermal model for summer conditions shown in Figure 5.6 does not vary greatly from the winter scenario shown in Figure 5.1. The major difference however, is that the South vent (as shown in Figure 4.4) of the room as well as the apex roof vent (the top of the channel) are now open to the atmosphere and subject to ambient conditions. From the model's perspective this means that the channel's boundary conditions change to incorporate the ambient surroundings.

Conservation of energy as applied to the roof

The conservation of energy applied to the roof is identical to that of winter as expressed in Equation 5.2, with the difference of the input values for the calculation of the amount of solar radiation being absorbed by the roof:

$$\dot{Q}_{abs} = \zeta_{summer} \alpha_f A_f \dot{G}_{summer} \quad (5.21)$$

The value of the summer geometric factor ζ_{summer} is calculated in Appendix B.2, while the input graph for summer incident solar radiation \dot{G}_{summer} can be found in Appendix B.2.

Conservation of energy as applied to the air channel

The channel is divided up into 9 control volumes as explained for the winter model. The energy balance applied to one control volume is the same as for winter and can be expressed by Equation 5.8. The boundary condition for the top of the channel is now ambient temperature, density and pressure, while the boundary condition for the bottom of the channel is still subject to the room or space conditions.

Conservation of energy as applied to the room

The room is treated as one control volume and it is assumed that thorough mixing of the air occurs within the space. The room receives or loses heat via mass transfer through the bottom of the channel, through the opening vent to the atmosphere as well as via conduction through the room walls to the environment and to the air in the channel. The room control volume is sketched in Figure 5.7.

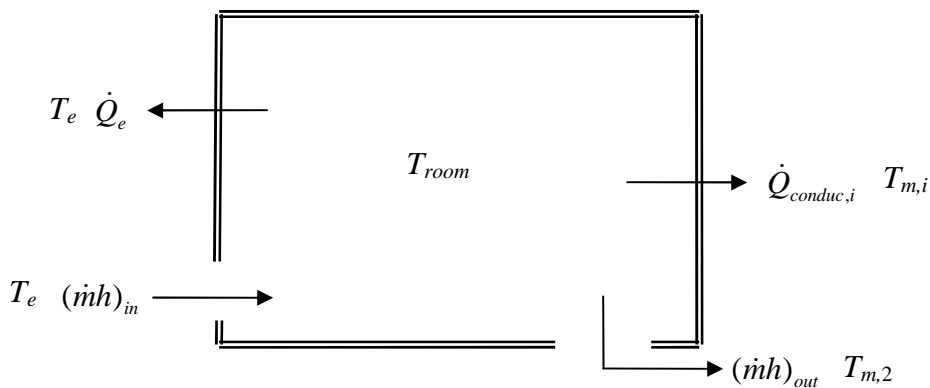


Figure 5.7: Sketch of summer room control volume

The conservation of energy applied to the room is the same as for winter as expressed in Equation 5.17, with the difference being the energy entering from ambient conditions of the environment in the enthalpy term. This can be expressed as:

$$\dot{Q}_{in} = (\dot{m}h)_{in} \quad (5.22)$$

Where $h = C_p T_e$ is the enthalpy term, C_p is the specific heat of the air, and T_e the ambient temperature.

Conservation of momentum

The conservation of momentum is applied to one control volume of the system as explained for the winter condition. The final equation is thus:

$$\frac{\Delta v}{\Delta t} = \frac{\sum_{i=2}^N (\rho DX g \sin \theta)_i}{\sum_{i=2}^N (\bar{\rho} DX)_i} - \frac{(P_{N+1} - P_0)}{\sum_{i=2}^N (\bar{\rho} DX)_i} - \frac{\sum_{i=2}^N \left(\frac{C_f \bar{\rho} v^2 2DXDZ}{2A_c} \right)_i}{\sum_{i=2}^N (\bar{\rho} DX)_i} \quad (5.23)$$

The channel is subject to different boundary conditions as explained previously and therefore the second term differs from the winter condition. In the second term, P_{N+1} and P_0 are the pressure terms at the top and bottom of the column of ambient air as shown in Figure 5.6. The pressure terms are calculated according to the temperature, density and height of the column of ambient air as:

$$P_{N+1} - P_0 = \rho_e g h_{column} \quad (5.24)$$

where $\rho_e = \rho$ at T_e .

The losses due to friction in the third term of Equation 5.24, require two additional values to the existing model for winter, for the sudden contraction and expansion of the air entering the room through the side vent. An additional length $L_{eq}=35D_{hyd}$ for the expansion into the room and $L_{eq}=16D_{hyd}$ for the contraction from the environment to the room opening is added to the length of the channel in addition to the existing frictional losses of the winter model. These simple additions are justified if the cross

sectional area of the opening into the room from the atmosphere equals that of the channel cross sectional area itself, which it does. The friction factor C_f is determined by the Reynolds number as explained earlier.

Accordingly the final equation for momentum conservation is expressed as in Equation 5.21 and can be solved by integrating around the natural circulation loop of Figure 5.6 to determine the velocity of the air flow at a certain cross section of the loop and finally the mass flow rate of the system.

5.2 Computer program

The equations given in the previous section were analyzed and calculated for a 24 hour time period in a Matlab program, using the explicit differencing method (Euler Method) with upwind conditions for the enthalpy, to calculate the new temperatures. The inputs to the program corresponding to the test-rig physical parameters and thermal characteristics are given in Table 5.1.

The input functions which vary according to the time of day include the incident solar radiation (on a horizontal plate), the ambient temperature, the relative humidity and the wind velocity. These are plotted in Appendix B.1 and B.2. This data was taken from the specific winter and summer day's readings from the weather station for the first day of Figure 4.8 and Figure 4.10 and curves were fit to the results. From this input data the dew point temperature of the ambient air and the emissivity and temperature of the sky during the day and night are calculated, as well as the amount of solar radiation striking the surface of the tilted roof according to the geometric factor ζ .

The program calculates a new set of control volume temperatures based on the previous time step's mass flow rate. The new temperatures are used to determine the new conditions (densities, mass and pressure) of the room air and channel air and to solve the momentum equation for the loop. A new air flow velocity is calculated for the chimney and the new mass flow rate. The new mass flow rate is used once again to calculate the new temperatures of the loop at different conditions and the process

repeats itself. This continues until a full day of 24 hours has been simulated. The winter and summer simulation programs can be found on the data CD of Appendix D.

Table 5.1: Input values for computer program

| <u>Variable</u> | <u>Symbol</u> | <u>Value</u> | <u>Units</u> |
|--|-----------------|-----------------------|-------------------|
| General | | | |
| Number of control volumes | N | 10 | |
| Gravitational acceleration | g | 9.81 | m/s^2 |
| Air gas constant | R | 287 | $kJ/kg\ K$ |
| Time | t | 24 x 3600 | seconds |
| Time step | dt | 0.5 | seconds |
| Roof | | | |
| Absorptivity constant | a_f | 0.2 | |
| Emissivity constant | ε_f | 0.2 | |
| Stefan-Boltzmann constant | σ | 5.67×10^{-8} | $W/m^2\ K^4$ |
| Specific heat of roof | Cp_f | 460 | $kJ/kg\ ^\circ C$ |
| Conductivity of roof | k_f | 43 | $W/m\ ^\circ C$ |
| Width of roof | DZ | 0.7 | m |
| Length of roof | L | 1.8 | m |
| Length of control volume | $DX=L/(N-1)$ | 0.2 | m |
| Roof thickness | ds | 0.0006 | m |
| Roof density | ρ | 7800 | kg/m^3 |
| Radiating surface of roof control volume | A_f | 0.14 | m^2 |
| Mass of roof control volume | Mf | 0.655 | kg |
| Inclination angle of roof from horizontal | θ | 45° | degrees |
| Air channel | | | |
| Total length of channel | L | 1.8 | m |
| Width of channel | DZ | 0.7 | m |
| Depth of channel | DY | 0.1 | m |
| Length of channel control volume | $DX=L/(N-1)$ | 0.2 | m |
| Inclination angle of channel from horizontal | θ | 45° | degrees |
| Cross-sectional area of control volume | A_c | 0.07 | m^2 |
| Volume of control volume | V_m | 0.014 | m^3 |
| Back of channel insulation conductivity | k_s | 0.03 | $W/m\ ^\circ C$ |
| Back of channel insulation thickness | t_s | 0.05 | m |
| Channel roughness | ξ | 0.6 | |
| Room | | | |
| Room diameter | Dr | 1.8 | m |
| Height of room | Dr | 1.8 | m |
| Cross-sectional area of room | $A_{c,r}$ | 2.54 | m^2 |
| Exposed area of room to back of air channel | A_s | 1.26 | m^2 |
| Exposed area to environment | A_r | 15.3 | m^2 |
| Room volume | V_r | 4.6 | m^3 |
| Average room insulation thickness | t_r | 0.1 | m |
| Room insulation conductivity | k_r | 0.03 | $W/m\ ^\circ C$ |

5.3 Results

5.3.1 Winter

The results from the simulation program for a typical sunny day in winter are shown in Figure 5.8. At a little after 12:00, notice that the solar chimney performs optimally, heating the room 5 °C higher than the ambient temperature.

As was seen for the experimental results (Figure 4.8 and Figure 4.9), the room and roof temperatures are strongly dependent on the incident solar radiation while the sun shines but then follow the course of the ambient temperature after sunset. Again it can be seen that the solar chimney also cools the room down to a lower temperature than that of ambient during the night, this being due to the roof cooling rapidly by radiation to the cold night sky (normally 10 °C or so lower than that of ambient) as seen in Figure 5.8. The maximum mass flow rate was experienced an hour after 12:00, and was equal to 0.00877 kg/s. Knowing the average density of the room and channel air this was calculated to be 26 m³ per hour. Taking the room volume as 4.6 m³ according to physical dimensions, this gives an air exchange rate of 5.7 per hour.

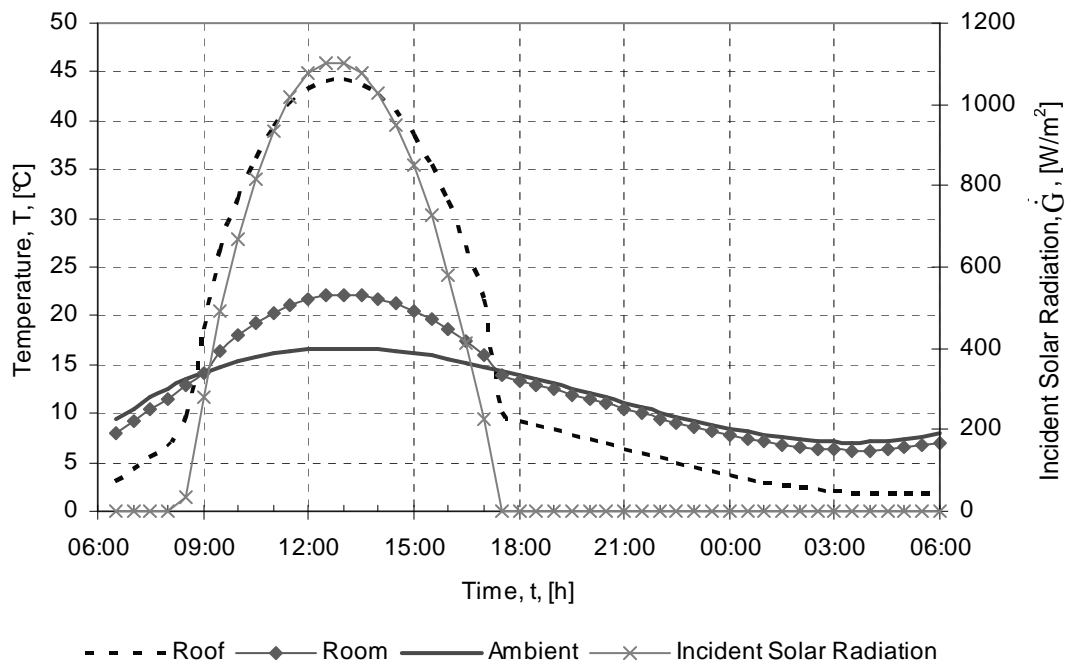


Figure 5.8: Simulation program results for a sunny day in Winter

For a cloudy day, all inputs remained constant with the exception of the incident solar radiation where the input function differs as shown in Appendix B.1. The results are plotted in Figure 5.9.

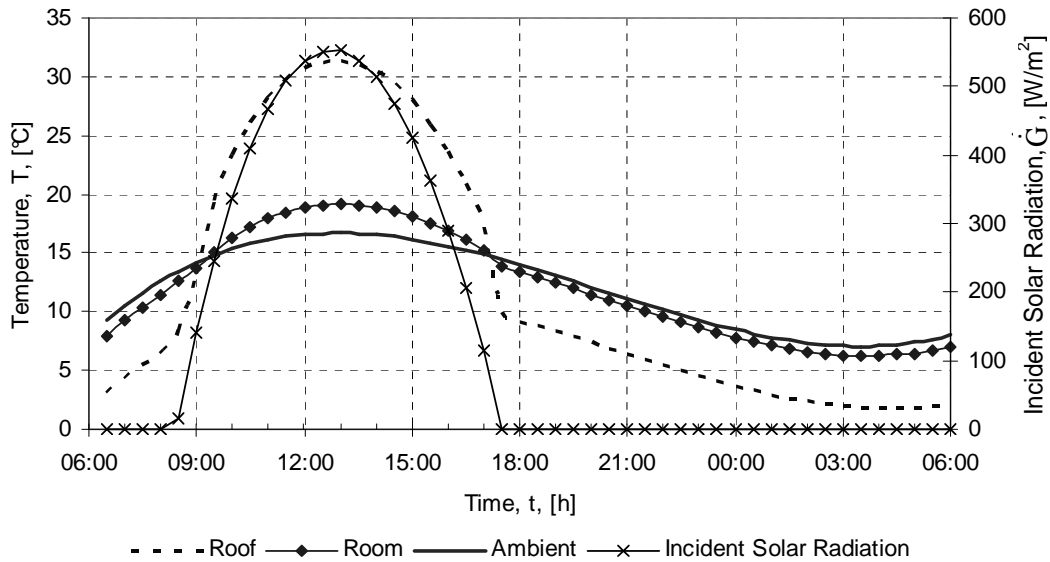


Figure 5.9: Simulation program results for a cloudy day in Winter

As expected, the room did not heat up as much as for a sunny day, but otherwise the two results do not deviate substantially. In the experimental results, the roof temperature varied frequently throughout the day due to the clouds and the haphazard intensity of the incident solar radiation. However, this erratic behaviour could not be precisely simulated using the simple function for solar radiation, so the program results are much smoother compared to the experimental results obtained.

The mass flow rate through the chimney is plotted for a sunny day in winter in Figure 5.10. As seen, the maximum mass flow rate ($\dot{m} = 0.00877 \text{ kg/s}$) through the channel corresponds with the peak solar radiation value. For a room with a volume of 4.6 m^3 , this gives an air exchange rate of 6.2 per hour which was considered the standard value for an office (Greenwood, undated). During the night however, reverse air flow occurs through the chimney channel, with mass flow rates being small. This means that at night and also during periods of low solar radiation, i.e. lower than 850 W/m^2 corresponding to a mass flow rate of 0.006 kg/s , the solar chimney is not effective in enhancing natural ventilation.

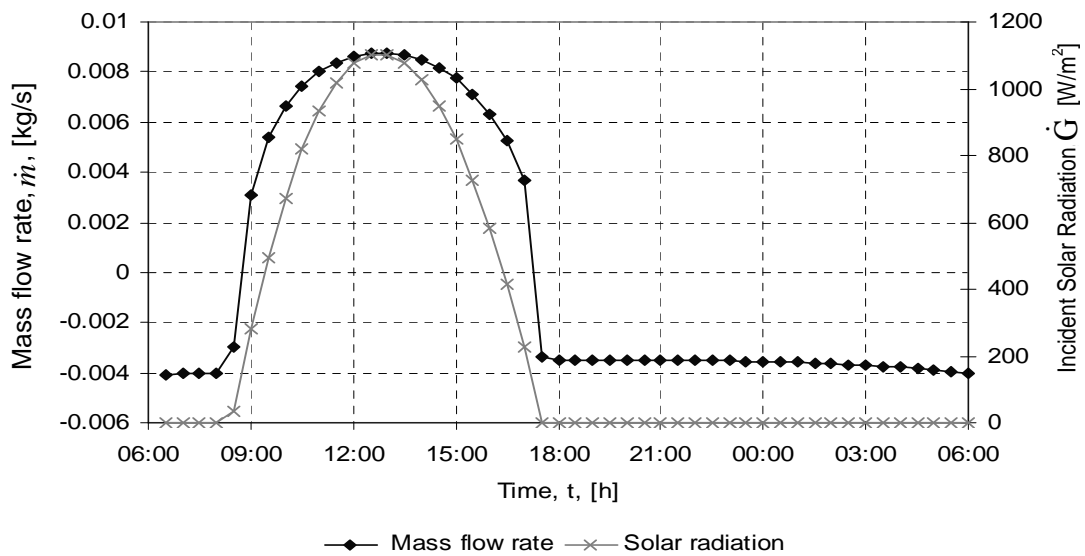


Figure 5.10: Mass flow rate and incident solar radiation for winter operation

5.3.2 Summer

For summer conditions two additional simulations were conducted for comparative purposes, in order to determine the effectiveness of the solar chimney concept in summer. The room with a solar chimney was compared to an identical sized room without a solar chimney but with the vents still open as well as to another identical sized room with no chimney and no vents open, i.e. a closed control volume. The three scenarios are illustrated in Figure 5.11.

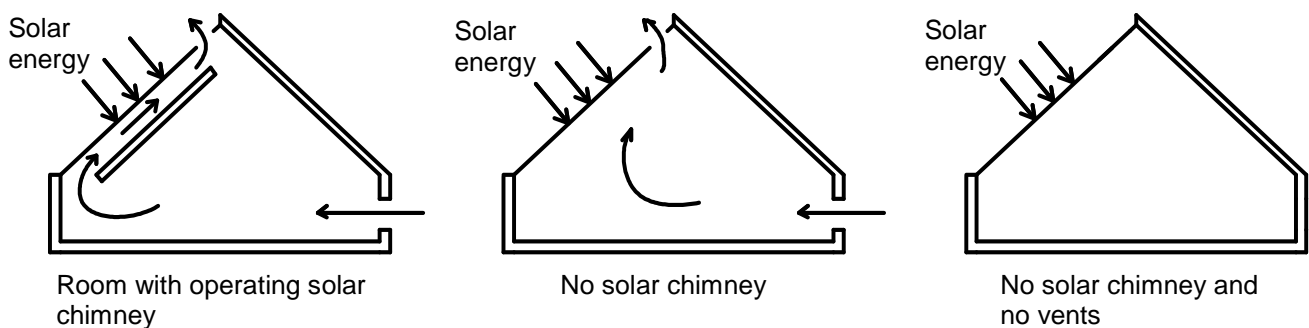


Figure 5.11: Three simulation models for summer operation comparison

Referring to Figure 5.11, the second model will still experience mass flow through the room due to the difference in buoyancy terms for the room air and the outside air, as the solar energy reaches the room and heats up the air. Since the last model has no vents open, no mass flow will take place and hence no energy transfer will occur via the enthalpy terms, but only through radiation and convection from the hot roof and conduction through the room walls to the environment. For the simulation program, all three models are subject to the same environmental conditions and solar radiation.

The simulation results for a typical sunny day in summer are plotted in Figure 5.12. All three results from the different simulation models as explained above are plotted on the graph and the effect of the solar chimney functioning is apparent.

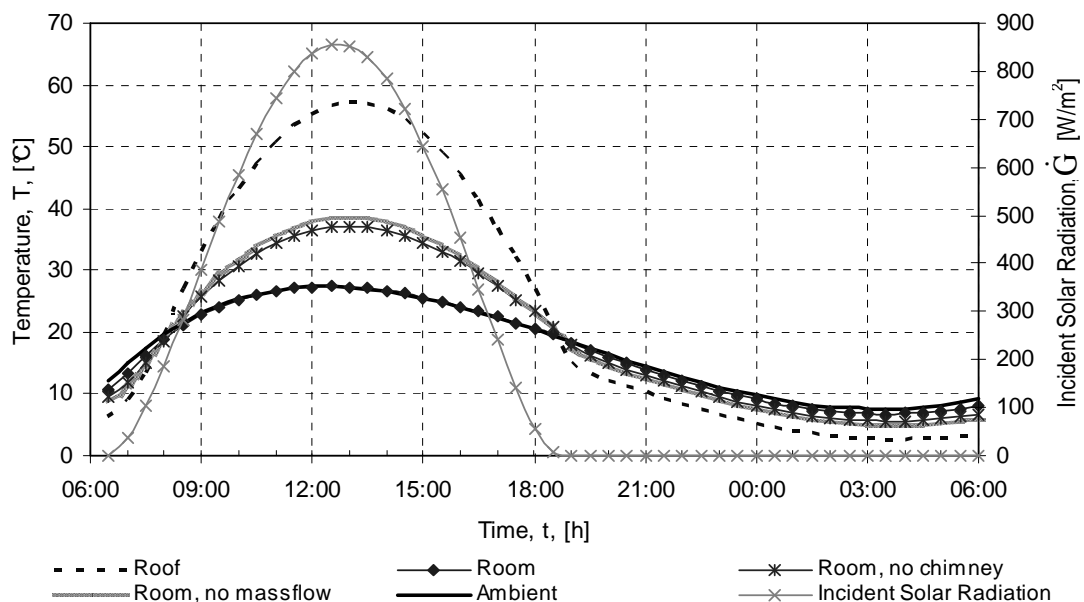


Figure 5.12: Simulation program results for a typical sunny day in summer

Firstly, referring to Figure 5.12, the incident solar radiation compared to winter is much higher and is also over a longer time period (12 hours) of the day. This ensures the higher roof temperatures seen in the figure. Secondly, the room (with the solar chimney) temperature matches the ambient temperature almost exactly since it is now exposed to the environment. The room with no chimney and the room with no air flow did not heat up as much as expected however. This is primarily due to the fact that radiation heat transfer inside the chimney channel and from the hot roof to the

surrounding inside wall surfaces for all three scenarios was ignored due to the complexity of the geometry of the structure.

A very simplified model and calculation to determine the effect of radiation heat transfer inside an enclosed polystyrene box with a corrugated roof is discussed in Appendix C. It was found that radiation from the roof and walls does play a significant role in heating up the air in the room, and should be considered in a more complex and accurate thermal model. Still, the difference in temperature between the room, the room without a chimney and the room without a chimney and no vents, is quite substantial even when ignoring radiation heat transfer inside the structure.

Since the aim of a solar chimney is to keep room air at ambient conditions during the summer and to enhance natural circulation, the chimney is measured against the other two rooms in terms of how well this was accomplished, i.e. the smaller the temperature difference between the room air and ambient the more effective the system. As seen in Figure 5.12, the solar chimney operates effectively throughout the day, keeping the room temperature at ambient conditions. During the hottest periods of the day the solar chimney ensures a 10 °C difference in temperature compared to the room without a chimney and for an enclosed room. Interestingly, the room with no airflow has almost the same temperature profile as the room with airflow and no chimney. This is explained in that the only difference in the thermal model of the former compared to the latter is the absence of the enthalpy terms which are dependent on the mass flow rates through the room, $(\dot{m}h)_{in}$ and $(\dot{m}h)_{out}$. The reason why there is thus so little difference between the two results is because the magnitude of the mass flow rates in the room without the chimney is so small, as will be discussed in the next paragraph.

The mass flow rates for the room with a solar chimney and the room without one were plotted along with the solar radiation in Figure 5.13. The maximum mass flow rate for the solar chimney room was found to be 0.01015 kg/s resulting in an air exchange rate of 6.6 per hour for the 4.6 m³ room at the hottest periods of the day.

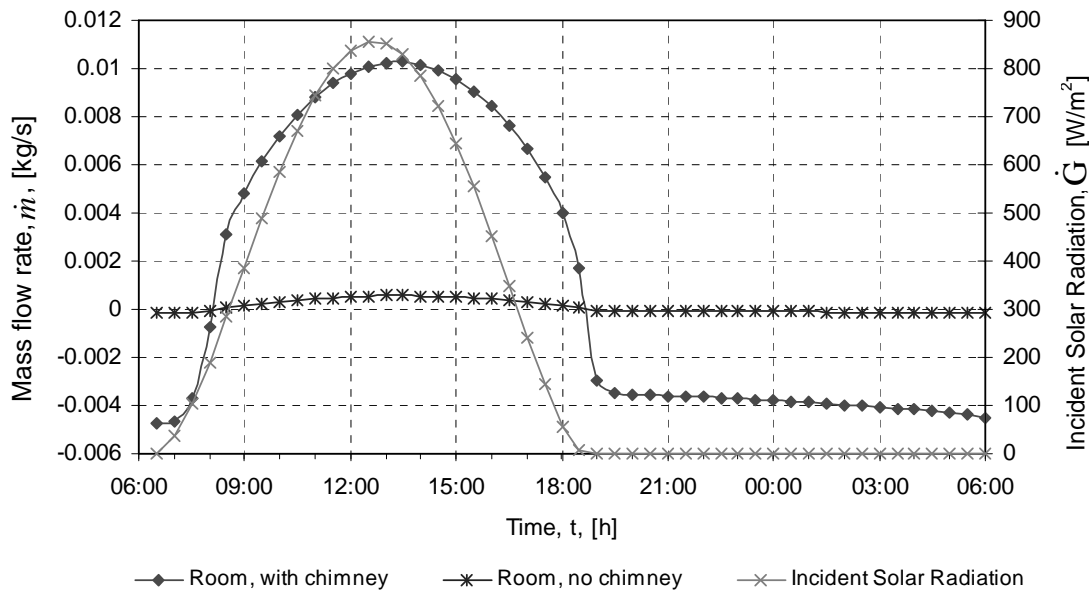


Figure 5.13: Mass flow rates for summer operation

This simulation result matches those of the analytical studies done by Bansal *et al.* (1993) as discussed in the literature review. This value is compared to the room with no chimney having a maximum mass flow rate of 0.0005 kg/s meaning an air exchange rate of only 0.33 per hour. Referring to the flow enhancing efficiency for summer operation defined in Chapter 2, the solar chimney increases natural circulation in this specific case by 95 %, but only during the period of peak solar radiation. This is a very large increase and thus illustrates that the solar chimney is an effective enhancer of natural ventilation, when subject to a high solar radiation intensity ($\dot{G} = 850 \text{ W/m}^2$).

As seen in winter operation as well, reverse air flow takes place (i.e. back down the chimney channel into the room) when the sun does not shine or during the night. The mass flow rates through the room during these periods are small, and do not contribute significantly in aiding natural ventilation.

5.4 Sensitivity analysis

5.4.1 Winter

A sensitivity analysis was performed for a variation of $\pm 50\%$ of the selected system variables from the base case scenario shown in Table 5.2. These include the room volume (which, as mentioned above requires the changing of one variable, the diameter D_{room}), the exposed roof radiation surface area, the absorptivity for the roof and the insulation thickness of the exposed walls of the room. The base case scenario was chosen to represent a room volume of 48 m^3 . This is ten times the size of the test-rig itself and about the size of a small loft of $4 \text{ m} \times 4 \text{ m} \times 3 \text{ m}$, and would represent a practical application of the solar chimney concept, the solar collector area was taken to be 6.2 m^2 which is five times that of the test-rig model. In fact it does not really matter what sizes are chosen for the base case for the sensitivity analysis since the aim is to determine the effect of changing certain key variables from the base case making this a comparative analysis. The winter base case computer simulation program can be found on the data CD of Appendix D.

The results are given in Table 5.2 below as a percentage variation of the system performance parameters. These are the total amount of heat absorbed by the roof depending on the size of the radiation area and the roof absorptivity α_f , over the 9 hour sun shining period (Q_{absorb}), and the total amount of heat energy reaching the room space over that same period ($Q_{in,room}$). This was calculated by summing the amount of heat energy flowing into the room every half hour, which was calculated by finding the temperature difference between the room temperature and ambient temperature for each half hour time step and multiplying this by the time elapsed (1800 seconds), the average mass flow rate and specific heat of that time step:

$$Q_{in,room} = \sum_{t=t_1}^{t_{max}} (\dot{m}_{avg,t})(C_v)(T_{room,t} - T_{ambient,t})\Delta t \quad (5.25)$$

The 'efficiency' of the system ($\eta_{thermal}$) was then defined by the input energy (the total amount of incident solar radiation falling on the roof during the 9 hour sun shining period) over this value explained above, $Q_{in,room}$. The maximum temperature of the room during the day ($T_{max,room}$) and the sum of the difference between the outside ambient air temperature and the inside room air temperature multiplied by the time

step for each of the hours of the nine hour sun period ($\Sigma(T_{amb}-T_{room})\Delta t$), was also recorded.

Table 5.2: Sensitivity analysis results for winter operation

| Variable | Q_{absorb} | $Q_{in,room}$ | $\eta_{thermal}$ | $T_{max,room}$ | $\dot{m}_{maximum}$ | $\Sigma(T_{amb}-T_{room})\Delta t$ |
|---------------------|--------------|---------------|------------------|----------------|---------------------|------------------------------------|
| | MJ | MJ | % | °C | kg/s | °C.hour |
| Base Case | 28.56 | 6.03 | 4.2 | 0.037 | 0.037 | 23.2 |
| $0.5A_f$ | -48 | -16 | +67.8 | -9 | +12 | -38 |
| $1.5A_f$ | +50 | +34 | -10 | +6 | +2 | +28 |
| $0.5\alpha_f$ | -50 | -40 | -40 | -12 | -12 | -53 |
| $1.5\alpha_f$ | +50 | +150 | +106 | +14 | +25 | +61 |
| Selective absorber | +300 | +18 | +218 | +70 | +30 | +343 |
| $\theta = 25^\circ$ | -3 | -30 | -31 | -27 | -27 | -11 |
| $\theta = 60^\circ$ | +21 | +50 | +23 | +10 | +27 | +35 |
| $0.5t_r$ | 0 | -4 | -4 | -10 | -8 | -38 |
| $1.5t_r$ | 0 | +48 | +48 | +8 | +25 | +33 |

The values for $\eta_{thermal}$ are low, possibly due to the energy lost through the walls of the room to the environment before heating up the room air. The most notable change in all the results occurs when varying the roof absorptivity α_f and the efficiency of the system increases substantial for higher values of α_f , especially for a selective absorber roof coating. The selective absorber aims to absorb as much solar energy as possible during the day with a high α_f value but at night has a very low emissivity constant ε_f and as such does not radiate all the absorbed heat to the cool sky at night.

What is also interesting is the efficiency of the system decreases for an increase in collector area and vice versa, which seems strange as more energy can be absorbed by the greater roof area. This could possibly be explained by the fact that the amount of solar energy being absorbed by the roof Q_{absorb} is reduced or increased by 50 % but the room's temperature $T_{max,room}$ still does not increase by much.

The tilt angle of the roof determines the amount of solar collector area exposed to the sun and therefore the amount of radiation absorbed. As seen, by tilting the roof at a steeper angle from the horizontal ($\theta = 60^\circ$) in the winter, when the sun is lower in the sky, exposes more surface area to the direct sun rays. Hence the efficiency and overall system performance increases. The opposite applies for a flatter angle ($\theta = 25^\circ$) when less area is exposed to the direct sun rays, decreasing the efficiency of the system. A flatter collector angle also results in a shorter vertical chimney height, which also decreases the mass flow rate through the system as determined by Equation 5.18.

Finally, wall thickness and insulation makes a slight a difference on the maximum temperature of the room. This emphasises the importance of insulating a room to improve temperature control and maintain a degree of thermal comfort.

5.4.2 Summer

The summer sensitivity analysis was conducted in a similar manner to the winter analysis, with the selected system variables being the exposed area of the solar collector or roof A_f , the absorptivity of the roof α_f , and the roof inclination angle θ . The base case scenario was chosen to represent a room volume of 48 m^3 , which is the same as the winter sensitivity analysis. The summer base case computer simulation program can be found on the data CD of Appendix D. Since the aim of summer operation of the chimney is not to heat the room up, the last two columns of Table 5.2 were not included in the summer analysis. The room insulation thickness does not play such a crucial role for summer as it does for the winter so the changing of this variable was omitted from the analysis.

Referring to Table 5.3, it was found that by increasing the collector area, reducing the volume of the room and increasing the absorptivity of the roof surface, that the flow enhancing efficiency was increased. The importance of using selective coatings on the roof is also evident by the large increase in the amount of energy absorbed by the roof and subsequent mass flow rate and efficiency.

Table 5.3: Sensitivity analysis results for summer operation

| Variable | Q_{absorb} | $Q_{in,room}$ | $\dot{m}_{maximum}$ | $\eta_{flow\ enhancing}$ |
|---------------------|--------------|---------------|---------------------|--------------------------|
| | MJ | MJ | kg/s | % |
| Base Case | 36.102 | 12.345 | 0.0488 | 92.5 |
| $0.5A_f$ | -50 | -35 | -28 | -3.7 |
| $1.5A_f$ | +50 | +27 | +20 | +1 |
| $0.5\alpha_f$ | -50 | -40 | -35 | -5 |
| $1.5\alpha_f$ | +50 | +37 | +29 | +2 |
| Selective absorber | +300 | +43 | +55 | +29 |
| $\theta = 25^\circ$ | +23 | -5 | -20 | -4 |
| $\theta = 60^\circ$ | -22.5 | -1 | +1 | -1 |

It is quite interesting to notice the effect of changing the inclination angle of the roof on the system parameters. By decreasing the roof angle in the summer ensures a greater collector surface area to the sun and subsequently a higher amount of energy absorbed. Yet because of the reduced perpendicular height of the column of air as shown in Figure 5.6, and the dependency of the buoyancy term on this column height, the less mass flow is induced which results in a lower efficiency. At a steeper angle, a smaller portion of the collector surface area is exposed to solar radiation so the chimney does not transfer heat to the air in the channel as efficiently either. This results in a smaller temperature and density difference between the air in the channel and the ambient air, which again determines the mass flow rate as depicted by Equation 5.23. It was found by Mathur *et al.* (2005) that the optimum tilt angle for a solar chimney collector to maximise the airflow rate through the chimney for a latitude of 35° is 50° from the horizontal.

6 DISCUSSION AND CONCLUSIONS

The direct comparison between experimental and analytical data for the temperatures of the room with the solar chimney for a typical sunny day in winter is represented by Figure 6.1. The values for the roof temperature for the experimental and analytical study compare favourably with one another except of course for the variability in the experimental curve caused by the rapid response of the test rig roof temperature to changes in wind velocity and solar intensity. There is a distinct time lag of up to 1 - 2 hours between the two sets of data for the room temperature, with the experimental data lagging the analytical data. There are at least two reasons for this, with the first being that the analytical model did not consider the thermal capacity of the polystyrene walls of the test-rig which, if taken into account, would have slowed down the response of the change of temperature of the room air. Secondly, it was difficult to match the experimental curve exactly for the ambient temperature for the input into the simulation program, so the results do not match up accordingly.

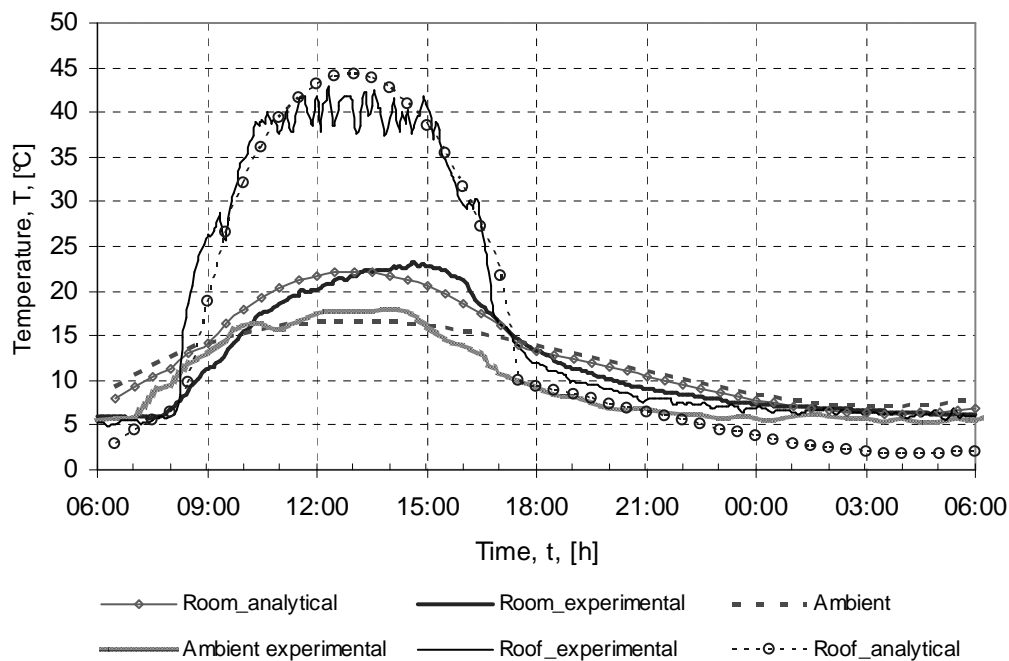


Figure 6.1: Comparison of experimental and analytical data for winter operation

The graph however, does illustrate that the two sets of data can be compared, meaning that analytical models can be used with confidence to predict the performance of solar chimneys relatively accurately. This is particularly useful when the wanting to determine the effect of changing certain system parameters will have on the performance of the solar chimney.

Regarding the experimental results for winter operation, when the aim is to heat up the attic space by re-circulating the warm air in the channel, this specific low-cost solar chimney design does not really perform substantially better when compared to any conventional loft containing a 50 mm layer of Isotherm™ roof insulation (Brits, 2007) against the roof. The chimney was able to warm the air up about 2-3 °C higher than the insulated room during the hottest periods of the day, and due to reverse circulation at night, the solar chimney also cooled the room down faster and had the lowest temperature of the three compartments during the night time period.

The amount of heat energy actually reaching the loft during winter operation is really quite small as found by the low thermal efficiency defined in chapter 2. It was found that the air exiting the top of the chimney was 8 °C higher than the entry temperature, yet the loft itself did not heat up to the same degree. It was concluded that most of the hotter air probably gathers at the very top of the loft near the apex of the roof and without some sort of mechanical means of ventilation, would not mix thoroughly with the air in the rest of the loft.

For summer operation, the experimental and analytical data for the solar chimney room air temperature are compared directly for a typical summer day in Figure 6.2. The results compare favorably with one another, except that again there is the slight time lag of the experimental values due to the heat capacity of the walls to retain a certain amount of heat, and that the input ambient temperature for the analytical model peaks slightly earlier than the experimental results.

The experimental data for the roof temperature is also lower than the roof temperature for the analytical study. This is probably due to the effect of wind on the convective heat transfer coefficient where the simulated wind profile for summer had slightly lower values than the real wind values for this day and also because the effect of if

radiation heat transfer in the chimney was not considered in the analytical model. It is therefore necessary to account for the influence of the radiation heat transfer and match the wind profile for that specific day more accurately in a future study. It is evident from Figure 6.2, however, that for summer operation, the solar chimney maintains the room air temperature close to ambient which is expected.

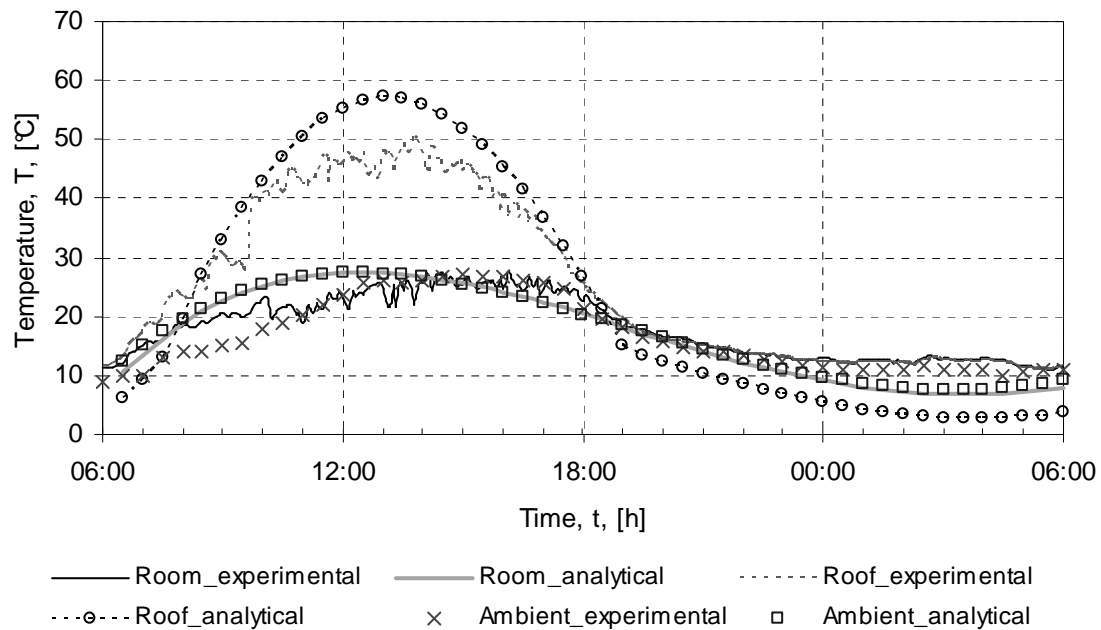


Figure 6.2: Comparison of experimental and analytical data for summer operation

With regards enhancing natural ventilation through the loft and ensuring a higher rate of air exchanges through the room, this solar chimney design was found to perform very well indeed, with flow enhancing efficiencies of 95 % for the hottest period of the day. This means that the solar chimney can effectively increase the mass flow rate through the loft by 95 % compared to a loft with only a vent at the apex of the roof. For this specific analytical study based on the solar chimney having a channel width, depth and length of 0.7 m, 0.1 m and 1.8 m respectively and a peak solar radiation of 850 W/m^2 it was found that an air exchange rate of 6.6 per hour was achieved for the 4.6 m^3 room at the hottest periods of the day, which agrees well with the literature.

During the night time however, the mass flow rate drops very rapidly, with air exchange rates reaching only 2.6 per hour on average. This is mainly due to the low

thermal capacity of the building materials making up the solar chimney, especially the collector itself which is a sheet of very thin corrugated iron with low thermal capacity and high conductivity. The collector therefore heats up or cools down rapidly according to the intensity of solar radiation, instead of retaining some of that absorbed heat and releasing it slowly during the night. In doing this, the collector could continue to release heat into the channel at night to ensure sufficient mass flow rates. This might also prove useful during winter operation, to continue to warm the loft space at night. It is concluded that for summer operation, this low cost design would work effectively during the hottest periods of the day in maintaining a degree of natural ventilation in a small loft.

The sensitivity analysis for both the winter and summer analytical studies provided valuable insight into improving the performance of the solar chimney. The two most important parameters when designing the system is the absorptivity of the solar collector surface and the tilt angle from the horizontal. It was found that by simulating a roof painted with a selective coating with absorptivity $\alpha = 0.8$ and emissivity $\varepsilon = 0.2$, that the thermal efficiency for winter operation increased by 200 % and the flow enhancing efficiency for summer operation increased by 29 %. A selective coating therefore increases the amount of solar energy absorbed by the surface but unlike a normal surface does not lose heat by radiation as quickly to the sky at night time, and so maintains the heat collected through the day for a longer period.

The tilt angle of the solar collector is another important aspect of the design. The tilt angle determines the quantity of collector area exposed to the direct sun rays, where, the higher the exposed area, the more solar energy is collected. Initially, the test-rig was simply built without any real thought as to the optimum angle of the roof, which is to enhance mass flow through the chimney channel *and* absorb as much solar radiation as possible. It was found however, that a 45° tilt angle for the latitude of location (35°) proved to be very close to the optimum angle of 50° as found by Mathur *et al.* (2005). This was further proved in the sensitivity analysis where it was found that the flow enhancing efficiency decreased for both a 25° and 60° tilt angle from the base case with a 45° tilt angle.

In general the study proved to be informative regarding the harnessing of solar energy using a non-conventional low-cost solar chimney design for passive thermal regulation. It was found that the corrugated iron performed well as a cost effective solar collector during the hottest and sunniest periods of the day but did not work effectively in transferring the collected energy to the room during the winter and as soon as the sun set for both the winter and summer operation, mainly due to the low thermal capacity of the corrugated iron and insulation material forming the back of the chimney.

7 RECOMMENDATIONS

Regarding recommendations and improvements to the study, the analytical model should include the effect of radiation in the chimney, and the thermal capacity of the walls of the loft space. Means of measuring the air velocities inside the chimney channel must be implemented. This could be done using a hot wire anemometer or tracer gas measurement, as this enables the evaluation of air exchange rates of buildings in real time, and further validates the analytical results obtained from the simulation model.

The simulation model can be made more realistic with the addition of heat sources within the loft space and including the effects of radiation heat transfer inside the chimney. Readings for summer operation should also ideally be conducted during the hotter months of the specific location, in this case January and February. The test-rig could also be built more realistically, with brick walls and a larger room volume which would also effect the thermal capacity and hence the response period of the experimental data as discussed earlier. CFD analysis of the test-rig would also provide valuable data to validate and compare with the experimental and analytical results.

To improve the general performance of the cost-effective solar chimney, the amount of solar energy absorbed should be maximized as far as possible. The corrugated roof can be painted with a selective absorber coating or simply a thick matt black paint to improve its collector efficiency. For a fixed collector, the optimum tilt angle should also be carefully considered before construction to ensure a maximum solar gain

averaged throughout the year and still ensuring sufficient chimney height to enhance the buoyancy effect for natural circulation.

For winter operation, the solar chimney was found only to be effective during the hottest parts of the day. The air is heated in the channel effectively but additional methods are needed to ensure mixing of the warm air accumulating at the top of the roof with the cooler air in the loft. The use of thicker walls or insulation in the loft itself would also help to retain heat accumulated during the day. At night the chimney actually cools the loft down to below ambient temperature, which is not desired. The use of a solar chimney to warm a loft during winter is thus not recommended, as much energy is lost to the environment at night. The chimney could still be used for natural ventilation, but additional methods of heating the living space must be sought.

To prolong sufficient mass flow rates during summer operation, the thermal capacity of the solar chimney materials should be increased. Methods include the use of thicker roofing sheets or tiles with higher thermal capacity than corrugated iron, or placing phase change materials (PCM) beneath the roof. PCM absorbs large amounts of energy while changing from one phase to another and releases this energy as heat at a later stage as the ambient temperature drops after the sun sets. Such a study was conducted by Kaneko *et al.* (undated) where it was found that the integration of PCM heat storage inside the solar chimney was available for natural ventilation in the evening and night, if the PCM completely melted in the daytime. The PCM used for their study was Sodium Sulfate Decahydrate " $\text{Na}_2\text{SO}_4 \cdot 10\text{H}_2\text{O}$ " commonly known as Glauber's Salt, chosen because it changes phase between 30 - 32 °C.

For the possible incorporation of this low-cost solar chimney into housing developments requires more work on achieving the optimum combination of cost and efficiency of the design. As it stands, the design is very cost-effective and easy to construct, but the practical results obtained from the analytical and experimental studies indicate it to be only a operationally feasible during hours of peak solar radiation. By continuing with these studies and improving the performance of the low-cost solar chimney with the recommendations given above, the design could be validated on a commercial scale and built into existing and new housing developments.

8 REFERENCES

Aboulnaga, MM, 1998, *A roof solar chimney assisted by cooling cavity for natural ventilation in buildings in hot arid climates: An energy conservation approach in Al-Ain city*, Renewable Energy, Volume 14, Issues 1-4, pp357-363, Elsevier.

Bansal, NK. Mathur, R and Bhandari, MS, 1993, *Solar chimney for advance stack ventilation*, Building and Environment, Volume 28, pp373-7,
<http://eprint.iitd.ac.in/dspace/bitstream/2074/2258/1/bansalso193.pdf> [June 2007].

Barenburg, AWT. 1974. *Psychrometry and Psychrometric Charts*, 3rd Ed, Cape and Transvaal Printers Ltd, Cape Town.

Batty, JC, and Folkman, SL., 1983. *Food Engineering Fundamentals*, p281, Wiley, New York.

Brits Nonwoven (Pty) Ltd., 2007, Official Website, Isotherm™ Thermal Roof Insulation, <http://www.brits.co.za/isotherm/isotherm.html>, [4 December 2007].

Çengel, YA, 2003, *Heat Transfer: A Practical Approach*, 2nd Ed, McGraw-Hill.

Davis Instruments Corporation, Official Website.
<http://www.davisnet.com/weather/index.asp>, [5 November 2007].

Greenwood Sales, undated, *Building Regulations*, p183,
http://www.greenwood.co.uk/media/pdfs/building_regs.pdf [23 October 2007].

Hamdy, IF, and Fikry, MA, 1998, *Passive Solar Ventilation*, Renewable Energy, Volume 14, Issues 1-4, pp. 381-386, 1998, Elsevier.

Hirunlabh, J, Wachirapuwadon, S, Pratinthong N, Khedari, J, 1999, *New configurations of a roof solar collector maximizing natural ventilation*, Building and Environment, Volume 36, Issue 3, pp383-391, 1 April 2001, Elsevier.

Kaneko, Y, Sagara, K, Yamanaka, T, and Kotani, H, undated, *Ventilation performance of solar chimney with built-in latent heat storage*, Department of Architectural Engineering, Osaka University, Japan,
http://intraweb.stockton.edu/eyos/energy_studies/content/docs/FINAL_PAPERS/4B-7.pdf [July 2007].

Kröger, DG, 2004, *Air-cooled Heat Exchangers and Cooling Towers: Thermal Performance Evaluation and Design*, Volume 1, Pennwell.

Lunde, PJ, 1980, *Solar thermal engineering: Space heating and hot water systems*, Wiley, New York.

Mathur, J, Mathur, S, Anupma, 2005, *Summer-performance of inclined roof solar for natural ventilation*, *Energy and Buildings*, Volume 38, Issue 10, October 2006, pp1156-1163, Elsevier.

Mills, AF, 1999, *Heat Transfer*, 2nd Ed, p571, Prentice Hall, New Jersey.

Miyazaki, T, Akisawa, A, and Kashiwagi, T, 2004, *The effects of solar chimneys on thermal load mitigation of office buildings under the Japanese climate*, *Renewable Energy*, Volume 31, Issue 7, pp987-1010, Elsevier.

Renewable Energy Annual, 1995, Energy Information Administration, p120, US Department of Energy, Diane.

APPENDIX A: THERMAL FUNCTIONS AND CALCULATIONS

Density of air at temperature T and pressure P

$$\rho = \frac{P}{(287.08)(T)} \quad (\text{A.1})$$

Dynamic viscosity μ of air at temperature T

$$\mu = 2.288 \times 10^{-6} + 6.2598 \times 10^{-8}(T) - 3.132 \times 10^{-11}(T)^2 + 8.150 \times 10^{-15}(T)^3 \quad (\text{A.2})$$

(Kröger, 2004)

Kinematic viscosity of air

$$\nu = \frac{\mu}{\rho} \quad (\text{A.3})$$

Heat Storage Capacity of air at temperature T

$$C_p = 1045.356 - 0.3161783(T) + 0.0007083814(T)^2 - 0.0000002705209(T)^3 \quad (\text{A.4})$$

(Kröger, 2004)

Conductivity of air at temperature T

$$k_{air} = -4.937787 \times 10^{-4} + 1.01809 \times 10^{-4}(T) - 4.62794 \times 10^{-8}(T)^2 + 1.2506 \times 10^{-11}(T)^3 \quad (\text{A.5})$$

(Kröger, 2004)

Prandtl number Pr

$$Pr = \frac{\mu C_p}{k_{air}} \quad (\text{A.6})$$

Reynold's number

The Reynold's number characterizes the flow of a fluid according to its velocity v , the distance its flows over a plate L as well as the density ρ and dynamic viscosity μ of the fluid. The Reynold's number indicates whether flow is either laminar or turbulent.

$$\text{Re} = \frac{\rho L v}{\mu} \quad (\text{A.7})$$

Convection heat transfer coefficient from roof to environment

For an inclined plate, the natural heat transfer coefficient is:

$$h_{up} = \frac{k_{air} Nu}{DX_f} \quad (\text{A.8})$$

DX_f is the length of the control volume. k_{air} is the conductivity of the air. Nu is the Nusselt number for natural convection and is calculated using the Raleigh number Ra and according to the magnitude of the Reynold's number Re of the ambient air flowing past the roof control volume as follows:

For the roof being cooler than ambient air the Nusselt number is $Nu = 0.27 Ra^{1/4}$.
 Otherwise, for the roof being hotter than ambient air, $Nu = 0.54 Ra^{1/4}$ if $Re < 1181$;
 otherwise $Nu = 0.54 Ra^{1/3}$

$$\text{where } Ra = \frac{g B \cos(\theta) (T_f - T_{air}) (DX_f)^3 \text{Pr}_{air}}{v_{air}^2}$$

g = gravitational acceleration

$$B = \frac{1}{T_{film}}$$

$$T_{film} = \frac{T_f + T_{air}}{2}, \text{ the average of the roof and ambient temperatures}$$

θ = roof inclination angle

Pr = Prandtl number of ambient air

Note that the Reynold's number is a function of the velocity of the ambient air i.e. depends on the input function of the wind velocity profile for a specific day.

Convection heat transfer coefficient from roof to channel air control volume

For the bottom side of a heated plate, the equation remains the same:

$$h_{down} = \frac{k_m Nu}{DX_f} \quad (\text{A.9})$$

However if the roof were to be hotter than the air in the channel then $Nu = 0.27Ra^{1/4}$.
 Otherwise for the roof being cooler than the air in the channel, $Nu = 0.54Ra^{1/4}$ if
 $Re < 1181$, otherwise $Nu = 0.15Ra^{1/3}$

where $Ra = \frac{gB \cos(\theta)(T_f - T_m)(DX_f)^3 Pr_m}{V_m^2}$

g = gravitational acceleration

$$B = \frac{1}{T_{film}}$$

$$T_{film} = \frac{T_f + T_m}{2}, \text{ the average of the roof and channel air temperatures}$$

θ = roof inclination angle

Pr = Prandtl number for air in channel

APPENDIX B: TIME DEPENDENT INPUT FUNCTIONS FOR COMPUTER PROGRAM

B.1 Winter program input functions

The input function for the solar radiation curve for the winter program was based on two time-dependent functions. The first function (Figure B.1) was obtained by fitting a continuous curve to the data measured by the solar radiation meter for the 21st of June, a sunny cloudless day. The reason measured data was used for the input program instead of recorded figures from tables was simply because it was desired to compare the experimental and analytical data directly, so the input solar radiation was chosen to match that of the experimental data on that specific day.

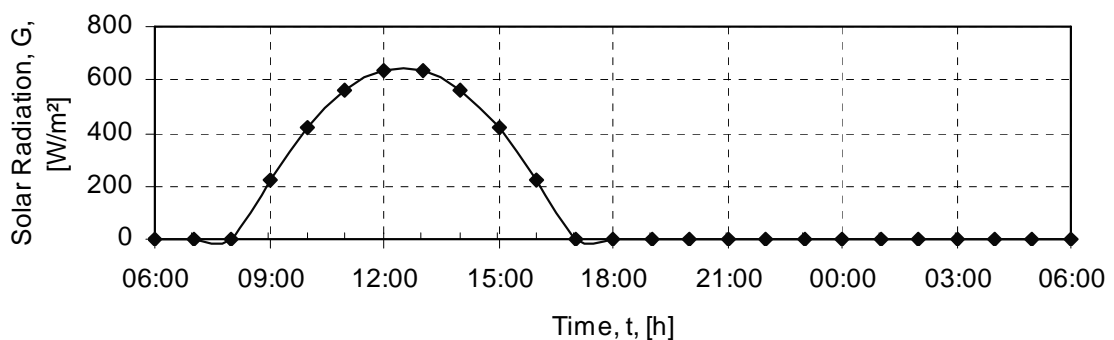


Figure B.1: Incident solar radiation on a horizontal plate in winter (sunny day)

Figure B.2 is a similar function obtained from data on the 11th of July, a cloudy day. However, the solar radiation sensor measures horizontal plate solar radiation only, which must first be corrected by a certain geometric factor depending on the time and position of the sun in the sky and the tilt angle of the solar collecting panel, in this case the corrugated roof.

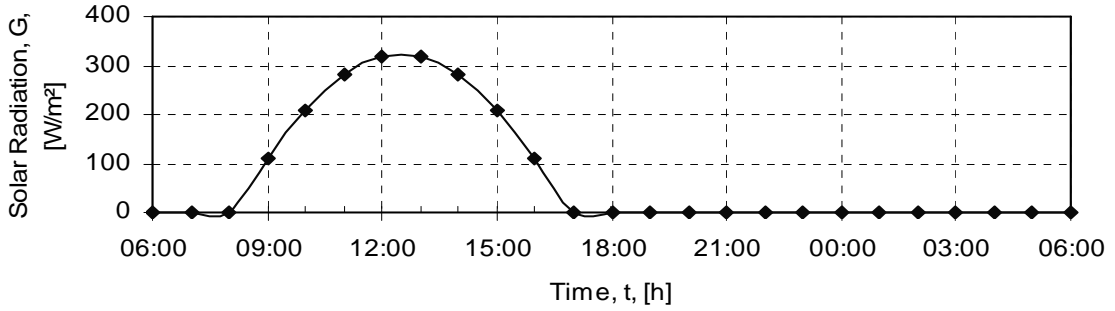


Figure B.2: Incident solar radiation on a horizontal plate in winter (cloudy day)

The winter solar magnification factor or geometric factor was calculated knowing the azimuth ψ and altitude ω angles of the sun for each hour of the day for the 21st of June (obtained from tables in Lunde, 1980), as well as the tilt angle θ of the roof itself.

Mathematically the geometric factor can be expressed by the relation:

$$\zeta_w = \frac{\cos(\omega)\cos(\psi)\sin(\theta) + \sin(\omega)\cos(\theta)}{\sin(\omega)} \quad (\text{B.1})$$

Since the roof angle for the test rig was fixed it was desired to determine the effect of tilting the roof to different angles in the sensitivity analysis hence the geometric factor was calculated for a 25° and 60° roof tilt angle as well. Figure B.3 plots the geometric factors for all three tilt angles corresponding to the time of day. Hence the input function to the winter simulation program is the multiplication of the geometric factor and the solar radiation on a horizontal plate.

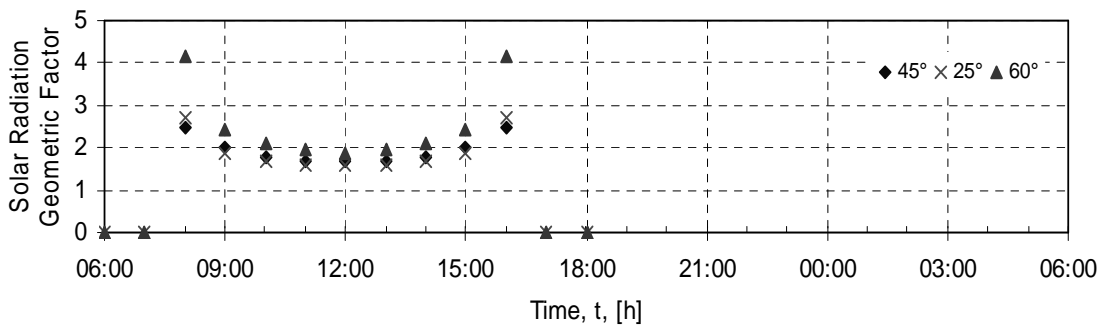


Figure B.3: Solar Radiation Geometric factor ζ_w for winter

Similarly, the ambient temperature, relative humidity and wind speed were obtained by fitting curves to measured data from the weather station and plotted in Figure B.4, B.5 and B.6.

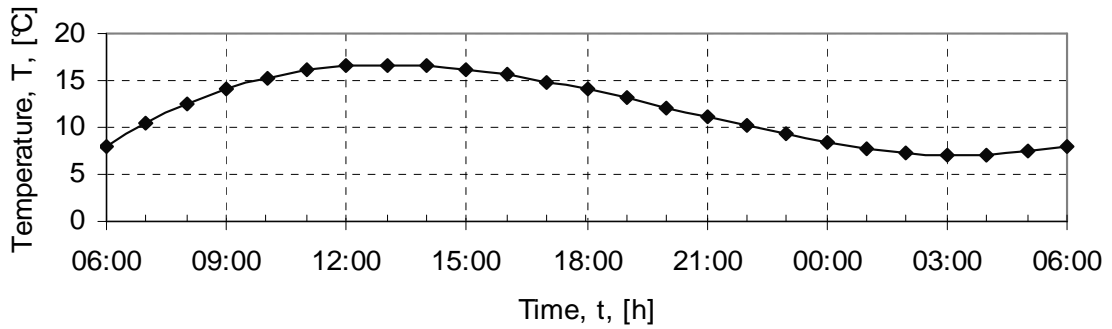


Figure B.4: Ambient air temperature over 24 hours

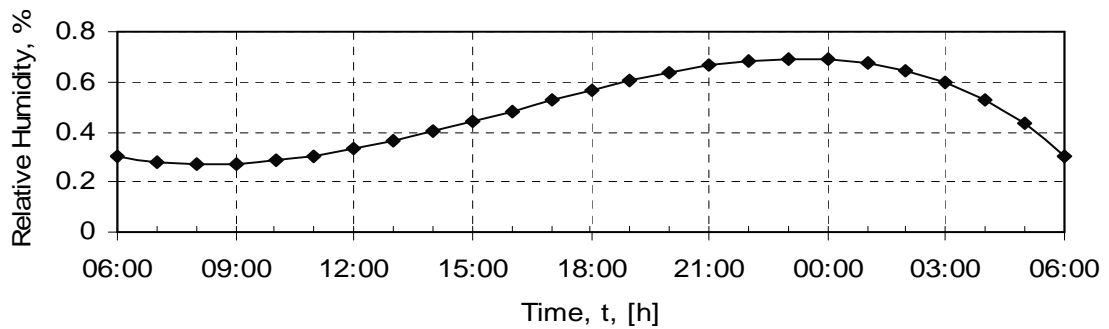


Figure B.5: Relative Humidity over 24 hours

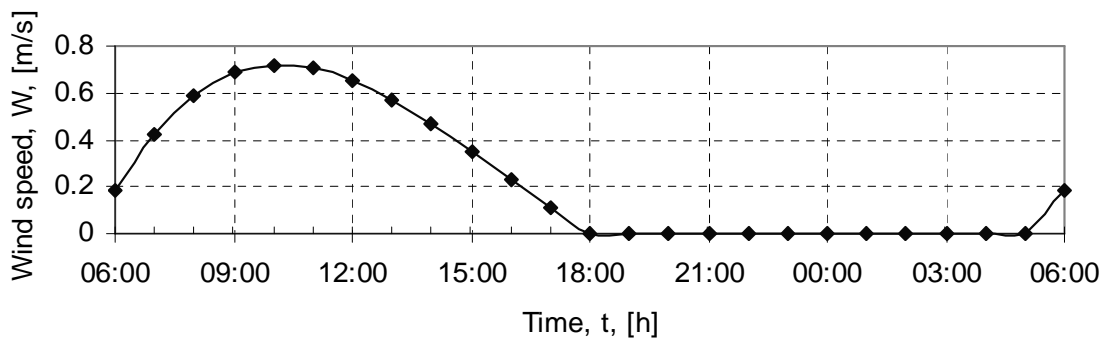


Figure B.6: Wind speed over 24 hours

B.2 Summer program input functions

The summer input functions for the solar radiation and geometric factor were calculated in the same way as explained for the winter simulation program. The horizontal plate radiation is plotted in Figure B.7 below.

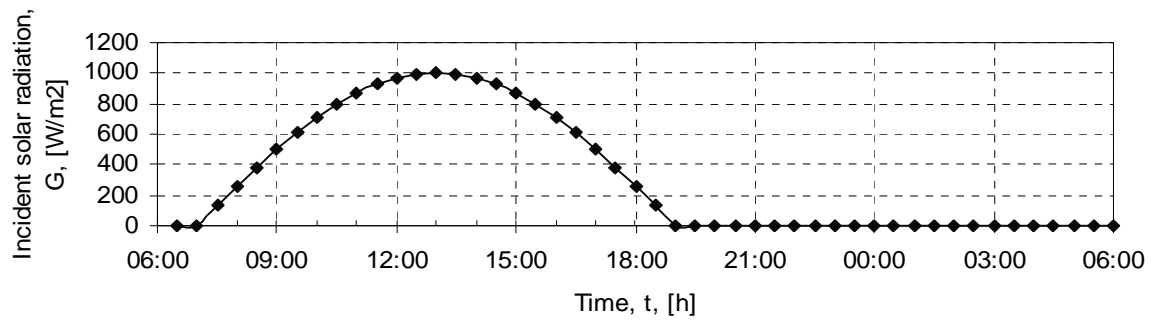


Figure B.7: Incident solar radiation on a horizontal plate for summer

Referring to Figure B.8, the summer solar geometric factor for the 45° roof angle is noticeably lower than that of winter because the tilted roof is exposing less of its surface area towards the sun's rays, compared to if it were lying flat. Similarly, more of the roof surface area is exposed to the direct sun rays when the tilt angle is 25° and less is exposed when the angle increases to 60°. Thus the horizontal plate radiation plotted in Figure B.9 is reduced accordingly.

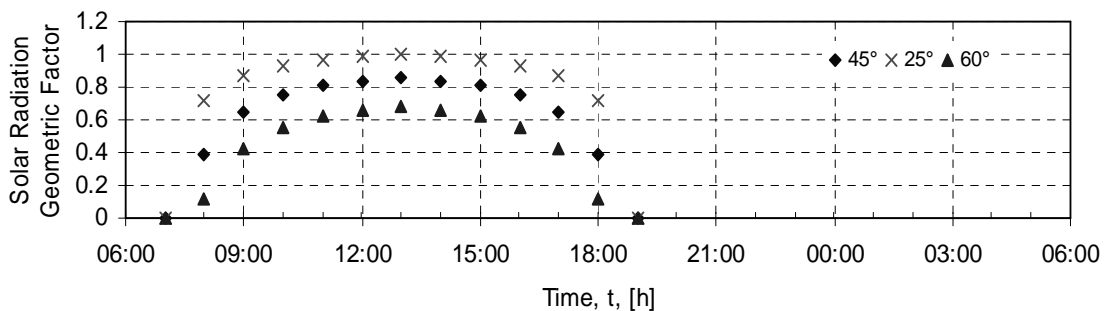


Figure B.8: Solar Radiation Geometric factor ζ_s for summer

Similarly, the ambient temperature, relative humidity and wind speed were obtained by fitting curves to measured data and plotted in Figure B.9, B.10 and B.11.

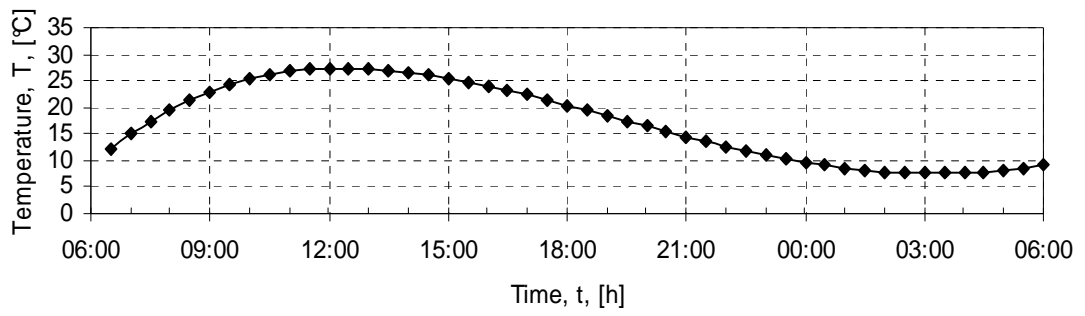


Figure B.9: Ambient air temperature for a typical day in summer

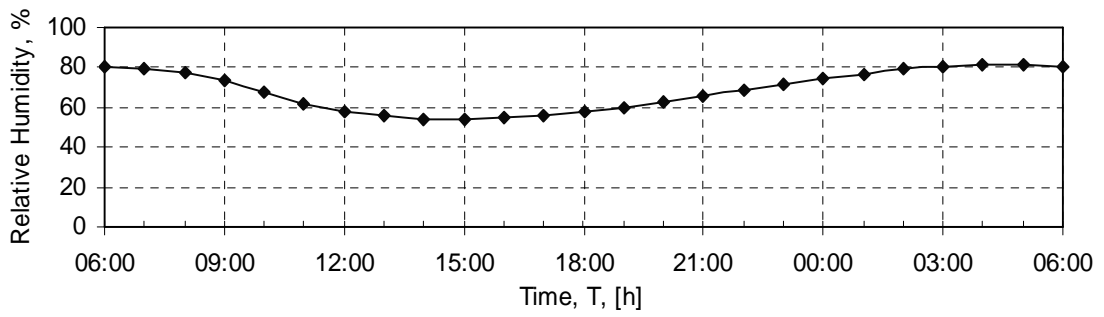


Figure B.10: Relative humidity over 24 hours

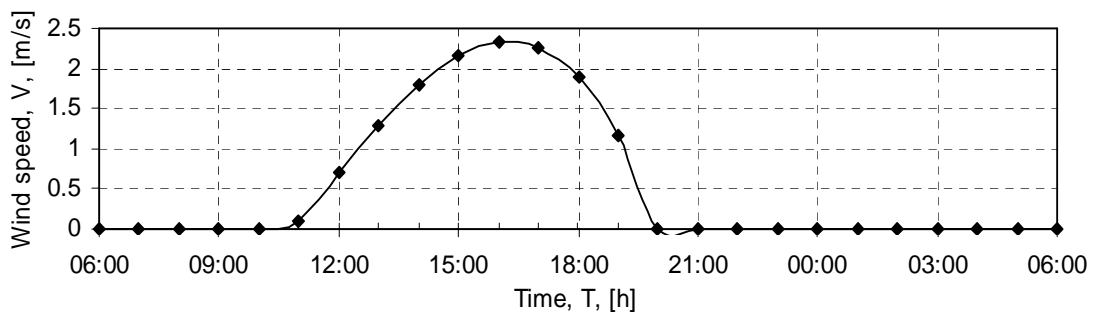


Figure B.11: Wind speed over 24 hours

APPENDIX C: RADIATION EFFECTS

The effect of radiation heat transfer from the roof to the walls of the room and from the walls to the room air were not incorporated into the simulation model due to the uncertainty and complexity associated with the structure of the room and the equations needed to model this mode of heat transfer. However, a small simulation program was written based on a simple polystyrene box with a corrugated roof lid as seen in Figure C.1 below to determine whether the heat being radiated from the hot roof onto the walls of the room, which then reradiate this heat back into the room space, does have a dominating effect on the temperature of the air in the room and the time period over which this would occur.

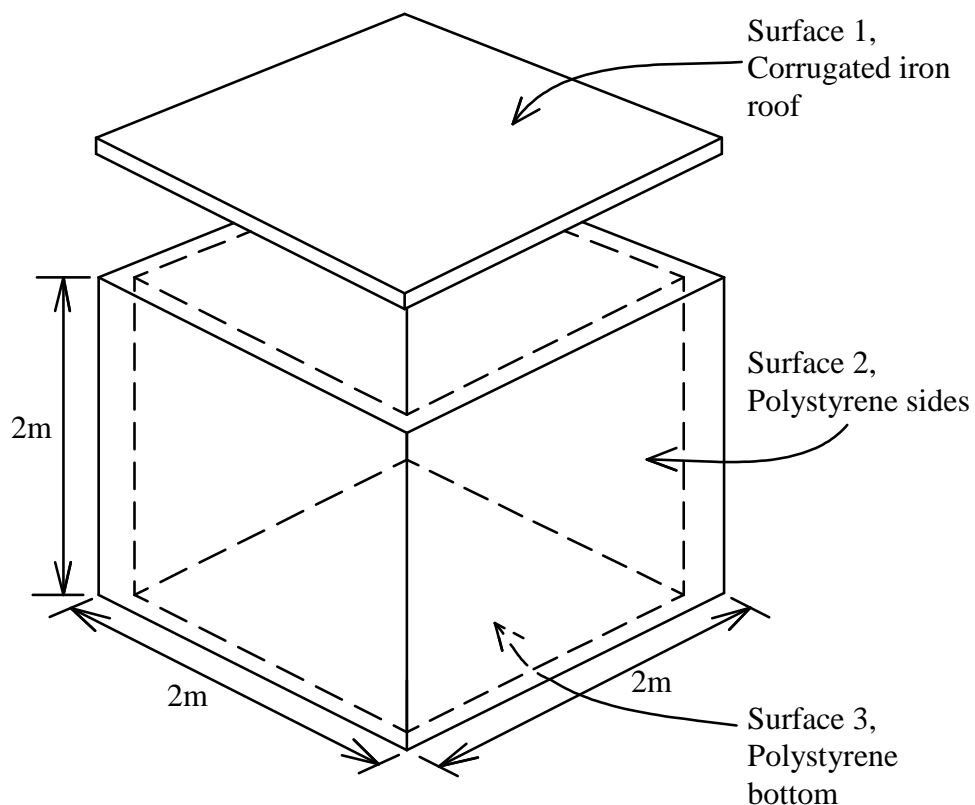


Figure C.1: Model for basis of radiation heat transfer calculation

Considering radiation heat transfer, the structure in Figure C.1 can be considered as an enclosure consisting of three opaque, diffuse gray surfaces; the top, the bottom, and with the sides forming one surface. The properties of such a surface are that they are opaque, diffuse emitters and diffuse reflectors and their radiation properties are independent of wavelength i.e. a grey surface (Çengel, 2003). Each surface can be considered isothermal and both the incoming and outgoing radiation are uniform over the surface. These surfaces have surface areas of A_1 , A_2 , and A_3 ; emissivities of ε_1 , ε_2 , ε_3 ; and temperatures T_1 , T_2 and T_3 as illustrated in Figure C.2. The air inside the box is stationary, so the only method of heat transfer from the roof to the sides and bottom walls and from the heated roof and walls to the air is via radiation and not convection.

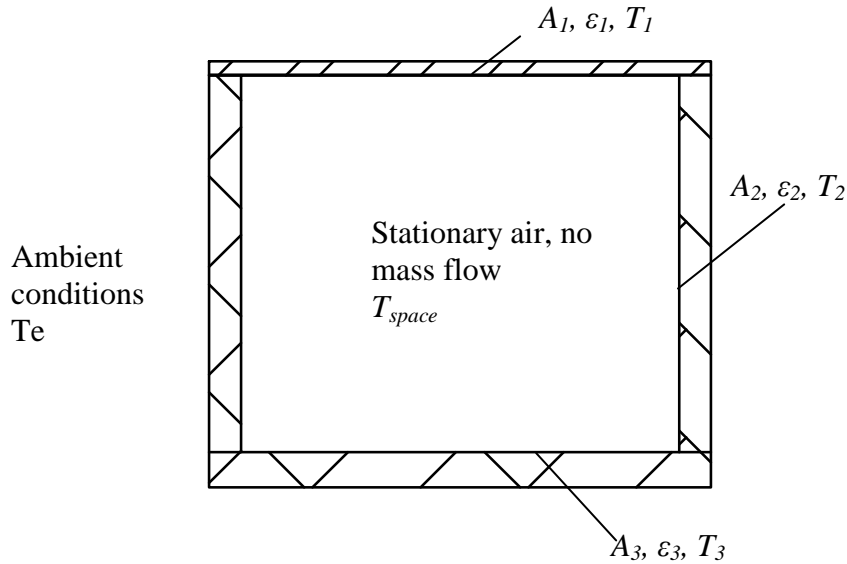


Figure C.2: Cross section of box for radiation effect calculations

During radiation interaction, a surface loses energy by emitting radiation and gains energy by absorbing radiation emitted by other surfaces. The total radiation energy streaming away from a surface, with no regard for its origin, is the radiosity J . Each surface has a surface resistance to radiation:

$$R_i = \frac{1 - \varepsilon_i}{A_i \varepsilon_i} \quad (C.1)$$

which is dependent on the area A_i and emissivity ε_i of that surface. In addition, when two surfaces radiate heat energy between each other, the rate of heat transfer is also subject to a space resistance:

$$R_{i \rightarrow j} = \frac{1}{A_i F_{i \rightarrow j}} \quad (\text{C.2})$$

where $F_{i \rightarrow j}$ is the form factor and represents the fraction of radiation leaving surface i that strikes j directly as a result of the relative orientation of the two surfaces to one another.

The radiation model above can thus be described by a network representation of net radiation heat transfer from surface to surface and is analogous to an electrical circuit of potential differences and resistances. The resistance network for the three-sided enclosure is shown in Figure C.3 below:

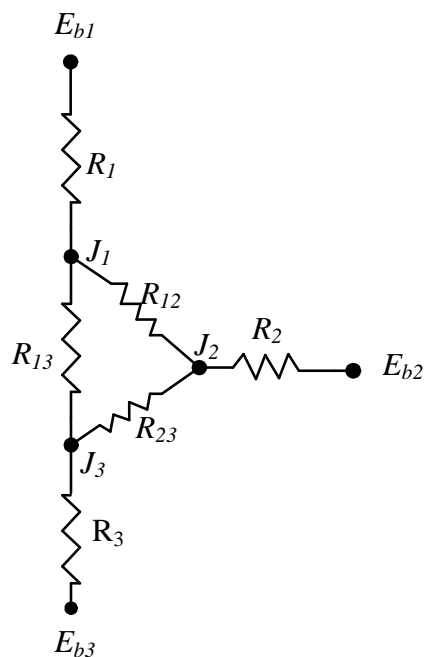


Figure C.3: Resistance network for radiation model

where R_1, R_2 and R_3 are the surface resistances denoted by:

$$R_1 = \frac{1 - \varepsilon_1}{A_1 \varepsilon_1}, \quad R_2 = \frac{1 - \varepsilon_2}{A_2 \varepsilon_2} \quad \text{and} \quad R_3 = \frac{1 - \varepsilon_3}{A_3 \varepsilon_3} \quad \text{respectively}$$

and R_{12} , R_{23} and R_{13} are the space resistances denoted by:

$$R_{12} = \frac{1}{A_1 F_{12}}, \quad R_{23} = \frac{1}{A_2 F_{23}} \quad \text{and} \quad R_{13} = \frac{1}{A_1 F_{13}} \quad \text{respectively.}$$

The three endpoint potentials E_{b1} , E_{b2} and E_{b3} are the blackbody emissive power of surface 1, 2 and 3 and for specified surface temperatures are equal to σT_1^4 , σT_2^4 and σT_3^4 respectively. Since these are considered known, the only unknowns are the radiosities J_1 , J_2 and J_3 which can be solved knowing that the algebraic sum of the 'currents' (net radiation heat transfer) at each node must equal zero. Mathematically this is represented as:

$$\begin{aligned} \frac{E_{b1} - J_1}{R_1} + \frac{J_2 - J_1}{R_{12}} + \frac{J_3 - J_1}{R_{13}} &= 0 \\ \frac{J_1 - J_2}{R_{12}} + \frac{E_{b2} - J_2}{R_2} + \frac{J_3 - J_2}{R_{23}} &= 0 \\ \frac{J_1 - J_3}{R_{13}} + \frac{J_2 - J_3}{R_{23}} + \frac{E_{b3} - J_3}{R_3} &= 0 \end{aligned} \quad (\text{C.3})$$

Once the radiosities are available the net rate of radiation heat transfers from each surface can be determined from:

$$Q_i = \frac{\sigma T_i^4 - J_i}{R_i} \quad (\text{C.4})$$

Concerning the geometry of the model in Figure C.1, the form factors were calculated as $F_{12} = 0.2$, $F_{13} = 0.8$ and $F_{23} = 0.2$ (Çengel, 2003). The areas are for $A_1 = 4 \text{ m}^2$, $A_2 = 16 \text{ m}^2$ and $A_3 = 4 \text{ m}^2$ and the emissivities for the roof or surface 1 is $\varepsilon_1 = 0.2$, and for the sides and bottom $\varepsilon_2 = 0.8$ and $\varepsilon_3 = 0.8$.

In order for the model to interact with the environment and the air in the enclosure, a step-wise approach was used. The roof was given a specified constant temperature of 60 °C and the sides and bottom wall temperatures T_2 and T_3 were guessed initially.

The problem was then considered only for radiation and the radiation equations of Equation C.1, C.3 and C.4 were solved to obtain the net heat transfer radiating from each surface.

The thermal model for the polystyrene box was considered as shown in Figure C.4. The roof surface was taken as one control volume with negligible heat capacity and material thickness, the air in the enclosed box was taken as one control volume, and finally the walls and floor of the box, were divided into 14 control volumes with increasing thickness from the exposed surface to the middle as illustrated in Figure C.4.

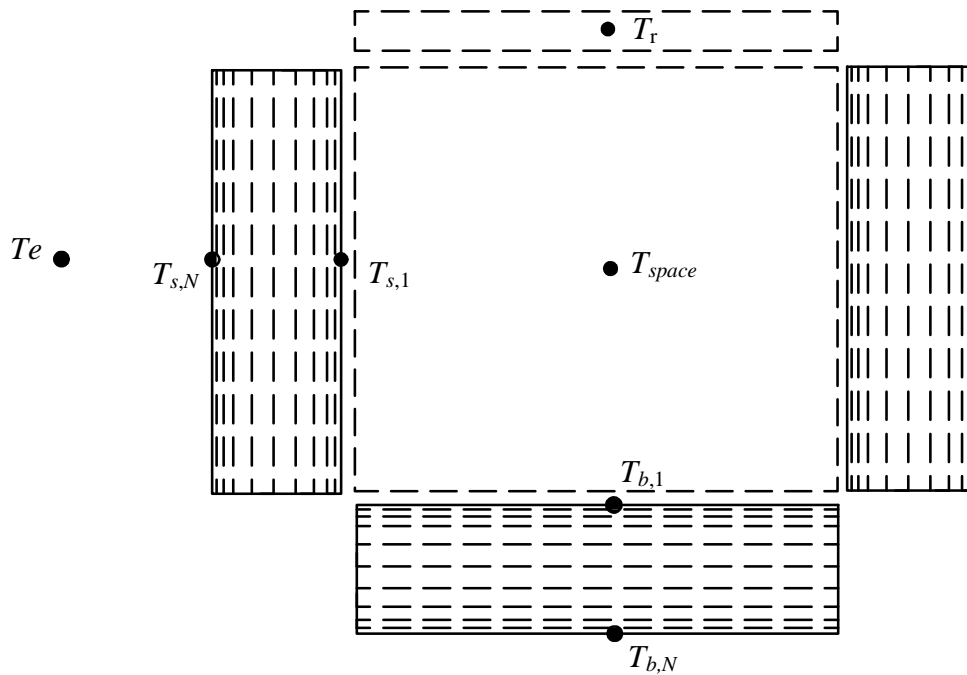


Figure C.4: Thermal model for polystyrene box

Conservation of energy applied to a boundary wall control volume

The boundary control volume for the bottom wall exposed to the inside of the box is shown in Figure C.5.

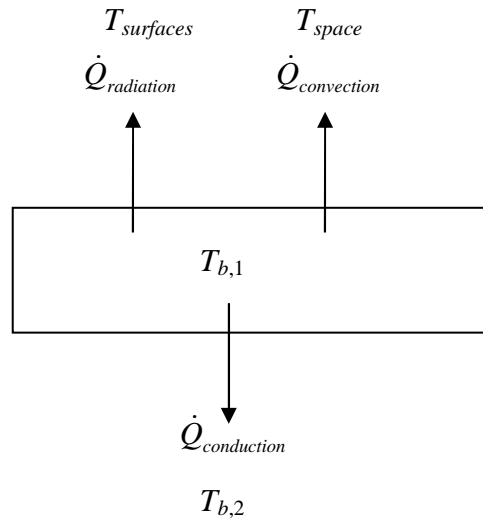


Figure C.5: Wall inner boundary control volume

Three modes of heat transfer take place in Figure C.5. Radiation heat transfer between the control volume and the side wall and roof takes place as explained previously and mathematically represented by Equation C.4. The convective heat transfer to the air in the space is:

$$\dot{Q}_{convection} = h_b A_b (T_{b,1} - T_{space}) \quad (C.5)$$

where h_b is the convection heat transfer coefficient for the bottom surface and taken to be 2, A_b is the bottom surface area exposed to the air in the space and essentially equal to $A_3 = 4 \text{ m}^2$.

The conduction heat transfer taking place between the boundary control volume and the next control volume in the wall is:

$$\dot{Q}_{conduction} = \frac{k_b A_b (T_{b,1} - T_{b,2})}{t_{b,1}} \quad (C.6)$$

where k_b is the conductivity of the polystyrene material and $t_{b,1}$ is the thickness of the control volume in question.

The change in temperature of the control volume over a given amount of time $\Delta t = t_2 - t_1$ is then given by:

$$T_{b,1}^{t_2} - T_{b,1}^{t_1} = \frac{-\dot{Q}_{convection} - \dot{Q}_{radiation} - \dot{Q}_{conduction}}{m_b C_v} \Delta t$$

Where m_b is the mass of the control volume and C_v the specific heat.

Conservation of energy applied to a boundary wall control volume exposed to the environment

Figure C.6 show the energy balance of the outer control volume of the bottom wall exposed to the environment.

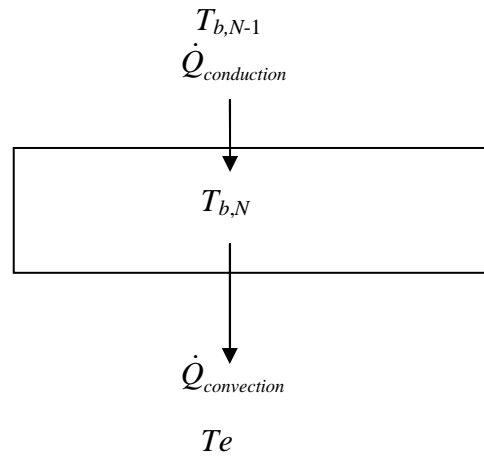


Figure C.6: Wall outer boundary control volume

Energy enters the control volume from the adjacent control volume via conduction as:

$$\dot{Q}_{conduction} = \frac{k_b A_b (T_{b,N-1} - T_{b,N})}{t_{b,N}} \quad (C.7)$$

Energy is also lost to the environment from the exposed outer surface by convection as:

$$\dot{Q}_{convection} = h_b A_b (T_{b,N} - T_e) \quad (C.8)$$

where T_e is the temperature of the air at ambient conditions.

The change in temperature of the control volume over a given amount of time $\Delta t = t_2 - t_1$ is then given by:

$$T_{b,N}^{t_2} - T_{b,N}^{t_1} = \frac{\dot{Q}_{conduction} - \dot{Q}_{convection}}{m_b C_v} \Delta t \quad (C.9)$$

Where m_b is the mass of the control volume and C_v the specific heat.

Conservation of energy applied to an inner control volume of a wall

Figure C.7 show the energy balance of the outer control volume of the bottom wall exposed to the environment.

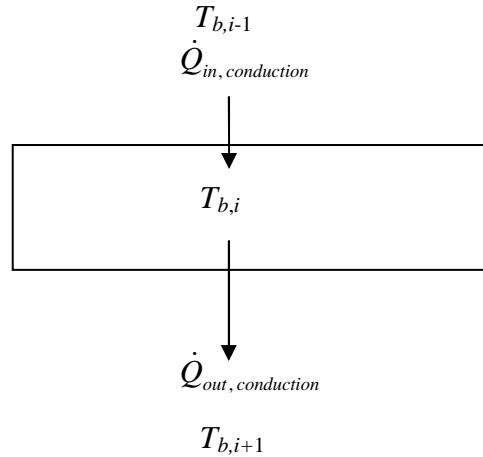


Figure C.7: Inner control volume of wall

The heat transfer from one control volume in the wall to the next is via conduction and expressed as:

$$\dot{Q}_{in, conduction} = \frac{k_b A_b (T_{b,i-1} - T_{b,i})}{t_{b,i-1}} \quad \text{and} \quad \dot{Q}_{out, conduction} = \frac{k_b A_b (T_{b,i} - T_{b,i+1})}{t_{b,i}} \quad (C.10)$$

Then the change in temperature of the control volume over a given amount of time $\Delta t = t_2 - t_1$ is then given by:

$$T_{b,i}^{t_2} - T_{b,i}^{t_1} = \frac{\dot{Q}_{in,conduction} - \dot{Q}_{out,convection}}{m_b C_v} \Delta t \quad (C.11)$$

The conservation of energy applied to the boundary control volumes for the inner and outer surfaces for the side walls results in equations similar to Equation C.4, C.5, C.6, C.7 and C.8, only that the subscript b is replaced with s for the side walls and the convection heat transfer coefficient has a value of 5.

Once the values of the control volume temperatures of the bottom and side walls are known, the new temperature of the air in the enclosed space can be calculated as follows:

$$T_{space,new} = T_{space} + \frac{\Delta t}{m_{space} C_v} (\sum \dot{Q}) \quad (C.12)$$

where $\sum \dot{Q} = h_s A_s (T_s - T_{space}) + h_b T_b (T_b - T_{space})$

Computer program

For the computer simulation, the above equations were calculated for one time step and the old values for the temperatures set equal to the new values for the new time step. The computer program was set to run for a two hour period as this was considered ample time to consider whether radiation plays a significant role in the third scenario for the summer simulation program with the room having no mass flow and no chimney. The radiation computer simulation program can be found on the data CD of Appendix D.

The ambient temperature was taken to be constant over the two hour period as 30 °C, and the roof was set at a constant temperature of 60 °C. The initial temperature of the room was taken as 20 °C. The temperatures of the air in the enclosure (T_{space}), surface 2 (T_{sides}) and surface 3 (T_{bottom}) and the constant temperatures of the roof

and the ambient air were plotted over a two hour period. The results are shown in Figure C.8.

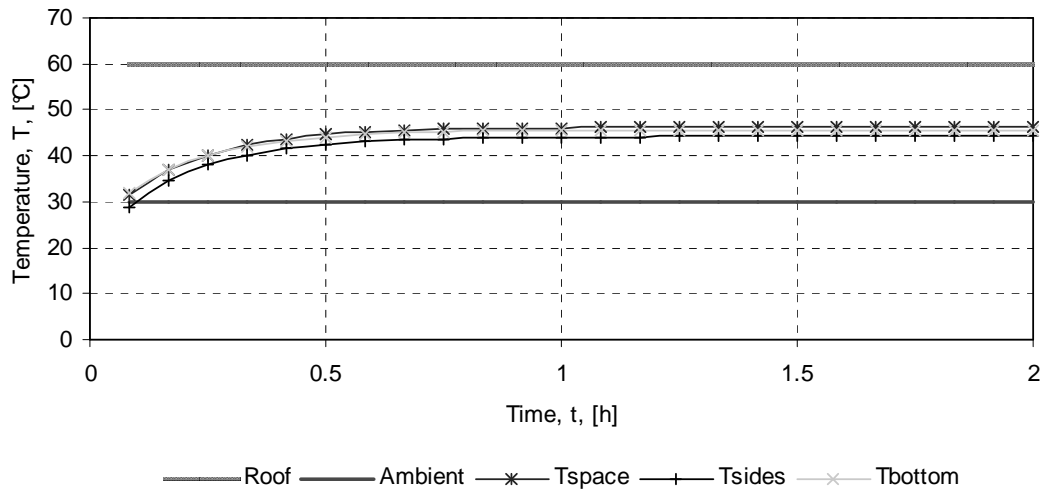


Figure C.8: Results for radiation heat transfer effects

It can be seen that after about half an hour the temperatures of the two surfaces and the air in the enclosed space reach an equilibrium temperature of 46 °C, which is 8 °C higher than the results obtained for the air inside the loft containing no solar chimney and no vents (Figure 5.11). This means that the effect of radiation heat transfer from the walls and floor are not negligible when heating up the air inside the loft for both the room with no vents and the room with vents, and should therefore not be ignored in the thermal model of the system. It is further concluded that radiation heat transfer inside the actual chimney channel should also be taken into account, to more accurately portray measured data.

APPENDIX D: DATA CD CONTAINING COMPUTER SIMULATION PROGRAMS

Contents of CD

- 1 Simulation programs for analytical study for Chapter 5
 - 1.1 Winter operation
 - 1.1.1 Main program
 - 1.1.2 Function files
 - 1.1.3 Base case for winter sensitivity analysis
 - 1.2 Summer operation
 - 1.2.1 Main program
 - 1.2.1.1 With chimney
 - 1.2.1.2 Without chimney
 - 1.2.1.3 Without chimney and without mass flow
 - 1.2.2 Function files
 - 1.2.3 Base case for summer sensitivity analysis
- 2 Simulation program for radiation effect calculation in Appendix C